

UNCLASSIFIED

AD NUMBER
AD918999
NEW LIMITATION CHANGE
TO Approved for public release, distribution unlimited
FROM Distribution authorized to DoD and DoD contractors only; Foreign Government Information; SEP 1973. Other requests shall be referred to The British Embassy, 3100 Massachusetts Avenue, NW, Washington, DC 20008.
AUTHORITY
DSTL, AVIA 6/24552, 17 Nov 2008

THIS PAGE IS UNCLASSIFIED



AD918999

ROYAL AIRCRAFT ESTABLISHMENT

β

MEASUREMENTS OF THE DRAG OF SOME CHARACTERISTIC AIRCRAFT
EXCRESCENCES IMMERSED IN TURBULENT BOUNDARY LAYERS

by

L. Gaudet
K. G. Winter

September 1973

AD No. _____
DDC FILE COPY

FOR OVERSEAS RELEASE OF INFORMATION
SEE INSIDE COVER

DDC
MAY 18 1974
RECEIVED
E2/10

A

CONDITIONS OF RELEASE

1. THIS INFORMATION IS RELEASED BY THE U.K. GOVERNMENT TO THE RECIPIENT GOVERNMENT FOR DEFENCE PURPOSES ONLY.
2. THIS INFORMATION MUST BE ACCORDED THE SAME DEGREE OF SECURITY PROTECTION AS THAT ACCORDED THERETO BY THE U.K. GOVERNMENT.
3. THIS INFORMATION MAY BE DISCLOSED ONLY WITHIN THE DEFENCE DEPARTMENTS OF THE RECIPIENT GOVERNMENT AND TO ITS DEFENCE CONTRACTORS WITHIN ITS OWN TERRITORY, EXCEPT AS OTHERWISE AUTHORISED BY THE MINISTRY OF AVIATION SUPPLY. SUCH RECIPIENTS SHALL BE REQUIRED TO ACCEPT THE INFORMATION ON THE SAME CONDITIONS AS THE RECIPIENT GOVERNMENT.
4. THIS INFORMATION MAY BE SUBJECT TO PRIVATELY-OWNED RIGHTS.

MAS Form 688 (revised 01/71)
Previously Mintech

12

(18) DRIC

(19) BK-39682

(14) RAE-TM-Aero-1538

ROYAL AIRCRAFT ESTABLISHMENT

(9) Technical Memorandum Aero 1538

Received for printing 11 September 1973

(6)

MEASUREMENTS OF THE DRAG OF SOME CHARACTERISTIC AIRCRAFT EXCRESCENCES IMMERSED IN TURBULENT BOUNDARY LAYERS.

by

L./Gaudet
K. G./Winter

(11) Sep 73

(12) 61p.

SUMMARY

Measurements are described of the drag of various forms of excrescence mounted on balances installed in the walls of the working section of the RAE 8ft x 8ft wind tunnel. The tests cover a range of Mach numbers between 0.2 and 2.8 (but not transonic) and a range of Reynolds number.

The excrescences tested include two-dimensional steps and ridges, circular cylinders and wings mounted normal to the surface, and holes and fairings. It is shown, for excrescences which are of height small compared with the boundary-layer thickness, that the scale effects on drag are well correlated in terms of the wall variables of the turbulent boundary layer, but that there is a dependence of drag on Mach number. For steps and ridges the effect of chamfering or rounding the upper corners was found to be beneficial at subsonic speeds but far less so at supersonic speeds. For circular holes the drag depends strongly upon the depth to diameter ratio. In an Appendix the oil-flow patterns obtained for a range of depth of circular holes are shown.

The fairings tested were either half-bodies of revolution with pointed or rounded ends or of square or rectangular section with pointed ends. The effects of different amounts of immersion of the bodies into the boundary layer were found in some cases by testing geometrically similar bodies of different sizes.

(51)

Amended version of paper presented at AGARD Specialists Meeting on Aerodynamic drag at Izmir 10-13 Apr 1973 with an Appendix on the flow in circular cavities.

240450

CONTENTS

	<u>Page</u>
1 INTRODUCTION	3
2 TEST ENVIRONMENT	4
3 EXPERIMENTAL TECHNIQUES	4
4 RESULTS	5
4.1 Steps, ridges and grooves	5
4.2 Circular holes	9
4.3 Rectangular holes	11
4.4 Circular cylinders	12
4.5 Stub wings	14
4.6 Fairings	15
5 CONCLUDING REMARKS	16
Appendix Visualization of flow in circular cavities	19
Symbols	23
References	24
Illustrations	24

Figures 1-36

Negs. C10483-10493

1 INTRODUCTION

The arrival on the aviation scene of supersonic transport aircraft with a high sensitivity in performance to drag at long-range cruise conditions and with an enormous development cost produced a demand for estimates of drag of higher accuracy than hitherto. For one of the ingredients of the drag, that of excrescences, very little information was available. Thus, although it was anticipated that any successful aircraft should be 'clean', it was difficult to assess what allowable tolerance should be placed, for example, on steps at skin joints, or to assess what were the drag penalties of essential excrescences such as aeri-als and pitot tubes. At about the same time it was becoming clear¹ that the drag of most current aircraft could have been lower if more attention had been paid to the avoidance of unnecessary excrescences. Even though there existed a considerable body of experimental evidence on the drag of most forms of excrescence at low speeds, mainly from the investigations of Wieghardt² and his co-workers, which has been collected together by Hoerner³, there was some doubt as to the application of the results over a wide Reynolds number range. There was thus a clear requirement for an experimental programme to measure drag of typical forms of excrescence on a surface over which flowed a turbulent boundary layer, for wide ranges of both Reynolds number and Mach number. Such a programme required a wind tunnel with variable density (an advantage not enjoyed by most of the previous workers in the field) and capable of operation at subsonic and supersonic speeds. Accordingly tests were made in the RAE 8ft x 8ft wind tunnel at Mach numbers between 0.2 and 2.8 with a Reynolds number range of about 10:1 at each Mach number. The range of Reynolds number was limited in some cases by the load ranges of the balances used and, for some configurations, the maximum Mach number was restricted to 2 because of unserviceability of the high-pressure section of the tunnel compressor. A shortcoming of the tests is that transonic conditions were not covered. To obtain high Reynolds number the walls of the tunnel were used, taking advantage of the knowledge⁴ already gained of the boundary layers there, and of the design of the strain-gauge balance used for measuring skin friction.

The excrescences tested included two-dimensional steps, ridges and grooves, representing defects in skin joints, cylinders and stub wings representing aeri-als and pitot tubes, circular and rectangular holes, and half bodies representing fairings over protrusions. These last were either half bodies of revolution with pointed or rounded ends or of square or rectangular cross-section with pointed ends.

2 TEST ENVIRONMENT

The drag of the various types of excrescence was measured by supporting them on balances (as described in the next section) which were mounted at four positions in the sidewalls, roof and floor of the working section of the RAE 8ft x 8ft wind tunnel. In this tunnel the roof and floor are flexible to provide variable supersonic nozzles. Since some 50 configurations of excrescence were contemplated, the small interferences, which may have existed between four excrescences tested simultaneously, were accepted in the interests of economic operation of the tunnel.

The turbulent boundary layer on the port wall of the tunnel has been investigated in great detail and its characteristics are known to be those for a flow with zero pressure gradient. Less complete (and less accurate) investigations have been made of the boundary layers on the other wall and on the roof and floor. Velocity profiles are not available for all four positions to confirm the symmetry of the flow but skin friction measurements - which were made of necessity to define the datum drag measured by the balances - show symmetry top to bottom and side to side. Characteristics of the boundary layers relevant to the analysis made of excrescence drag are shown in Figs.1, 2 and 3.

3 EXPERIMENTAL TECHNIQUES

The excrescences were mounted on strain-gauge balances of design similar to that previously used for skin friction measurement⁴. Two of the balances, used for the smaller excrescences, were capable of measuring drag loads up to 1.8 kg and two, for the larger excrescences, had ranges up to 18 kg. A balance with the larger range (the range depended only upon the size of the supporting flexures) is shown in Fig.4. It differs from the original design in having four flexures rather than three in an effort to reduce the sensitivity of the readings to temperature differences between the front (friction) plate and the rear (mounting) plate. All four flexures are nominally of the same stiffness in the fore-and-aft direction but strain gauges are mounted only on two of them. The other two flexures are of square section, to give a reduced stiffness in the transverse direction (compared with the main flexures), so reducing transverse stresses caused by temperature changes. Nevertheless some sensitivity to temperature remained and corrections have been applied to the readings on the basis of a calibration which used the difference in the indicated stresses of the two main flexures as a measure of temperature difference between the front and rear plates.

The primary load calibrations of the balances were made *in situ* before and after each test, by means of weights suspended on a fine cord attached to the centre of the friction plate and passing over a large diameter balanced pulley. For the balances mounted in the roof and floor the balance readings for zero load were adjusted to account for gravitational forces arising from the change of slope of the surfaces with change of setting of the nozzle shape with Mach number.

A further correction has been made to the readings to eliminate forces due to the pressure variations around the edge of the friction plate where twelve pressure tapings were provided.

The three-dimensional excrescences were mounted directly on (or, in, for the case of holes) the front plate of the balance. For the two-dimensional forms, the excrescence was continued on the sidewall to avoid end effects. This was straightforward for ridges, but for steps it necessitated a fairly large fairing attached to the tunnel wall either upstream or downstream of the balance centre-line across which the step was formed. It was checked, by making measurements with both upstream and downstream fairings in position, as shown in Fig.5, and with a packing piece on the balance plate to maintain a continuous flush surface, that the local skin friction was not affected by the presence of the fairing.

The drag of an excrescence is obtained as the difference between the force on the balance with an excrescence present and the force on the clean balance in the same flow conditions. Consequently the results presented include the effect of changes in skin friction on the balance but not on the tunnel wall.

In the present summary paper space does not permit a detailed assessment of the potential accuracy of the measurements of the drag of many different excrescences at many different conditions. However, as a rough assessment of accuracy a possible error of about 5% of the local skin friction on the balance plate may be taken for the small balances at average Reynolds numbers, and ten times this for the large balances.

4 RESULTS

4.1 Steps, ridges and grooves

The heights of these forms of excrescence were small compared with the boundary-layer thickness. The appropriate parameters on which the flow may be expected to depend are therefore those of the inner region of the boundary layer, as employed for example in expressing the calibrations of surface devices

used to determine skin friction. Accordingly a drag parameter, drag per unit frontal area divided by surface shearing stress, is regarded as a function of a roughness Reynolds number, i.e. $C_D/c_f = f(h^+)$, with $h^+ = u_\tau h/\nu$, where C_D is the drag per unit area divided by the freestream kinetic pressure, c_f is the local skin-friction coefficient in the absence of the excrescence, h is the height or depth of an excrescence and u_τ and ν are the friction velocity and kinematic viscosity based on wall conditions. Fig.6 shows that, for a forward-facing step at a given Mach number, there is a unique line (within the scatter due mainly to fluctuations in readings) indicating a linear variation of this drag parameter with the logarithm of h^+ . The drag parameter increases, for a given value of h^+ , with increase of Mach number up to $M = 1.4$ or a little beyond, but is apparently independent of Mach number for further increase of Mach number up to the maximum, 2.8, at which the tests were made. The values of h^+ show that in all the conditions of the tests the tops of the steps are within the logarithmic region of the undisturbed turbulent boundary layer. It may be expected that the variation of the drag parameter with h^+ will change for very small step height in a way analogous to the change in character of the velocity profile in the blending region and sublayer of the boundary layer. In this connection it is worth remarking that the behaviour is different from that for distributed roughness in that there appears not to be a critical height below which no drag increment occurs. Although the present results define a logarithmic variation only for relatively small heights of step, the results of Good and Joubert⁵ for the drag of the forward face of a fence at low speeds show that the same variation holds even when the height of the fence exceeds the boundary-layer thickness. This variation implies that neither the 'independent drag coefficient' of Hoerner³, in which the kinetic pressure used in forming the drag coefficient is the mean over the height of the step in its absence, nor a drag coefficient based on the velocity at the top of the step, is constant over a range of height. In the range of h^+ from 40 to 1000 the former varies at low speed between 0.36 and 0.68 and the latter between 0.17 and 0.41.

A detailed survey of previous work has not been made but similar logarithmic variations can be deduced from a selection of measurements from other sources. The results of Wieghardt² at low speeds are shown on Fig.6 and yield somewhat lower values of drag. The results of Good and Joubert⁵ give values of drag about 50% higher than the present results. They are, of course, for a different configuration and were obtained from pressure measurements, thus excluding changes in skin friction on the datum surface.

At supersonic speeds drag deduced for example from the pressure measurements of Kepler and Bogdonoff⁶ and Vas and Bogdonoff⁷ at Mach numbers of 2.92 and 3.85 is roughly in accord with the present analysis. The calibration of razor-blade surface pitot-tubes expressed in the form of Fig.6 also is roughly in agreement. The measurements of Czarnecki *et al.*⁸ of the drag of repeated steps at $M = 1.61$ on a body of revolution give lower drag, as would be expected qualitatively because of interference between the steps.

The effect of rounding the upper corner of the steps is shown in Fig.7. The full and broken lines are for values of h^+ of 1000 and 200 respectively. It can be seen that at subsonic speeds a small amount of rounding produces worthwhile reductions in drag. For example the drag is roughly halved for a radius equal to one third of the height. For supersonic speeds the drag reduction is much smaller. A similar difference between the behaviour at subsonic and supersonic speeds occurs for the effect of chamfering as shown in Fig.8. This difference in behaviour is perhaps not surprising if the effective wedge angle, which would give the measured drag of a plain step in inviscid flow, is evaluated. At $M = 2$ and $h^+ = 1000$ this angle is only 13 degrees. Thus, if the flow attaches on a rounded step at the same angle, the effective height might be expected to be changed by a factor equal to the cosine of this angle for a radius equal to the step height, i.e. an effective reduction of 3%. The effect of a chamfer would not be expected to be very great until the angle was reduced to a value of the same order as the effective separation angle.

The drag of rearward-facing steps has been plotted in the same way in Fig.9. Mean lines only are shown to avoid confusing the figure. The scatter of the experimental points is slightly greater than in Fig.6. The measurements at $M = 1.7$ and 2.0, which were taken in a different set of tests from the body of the results, show some inconsistency with the other results. The drag parameter varies linearly with the logarithm of h^+ as for forward-facing steps but the variation with Mach number is different. At a given value of h^+ the drag parameter increases with increase of Mach number from low speeds to reach a maximum at about $M = 1.4$ and then falls again at higher Mach numbers. This type of behaviour has been noted previously by Hastings⁹ in his measurements of base drag. His results at supersonic speeds are in fair agreement with those in Fig.9. As for forward-facing steps, the results of Ref.8 give lower drag. At low speeds the results agree well with those of Wieghardt² but not with those of Tani *et al.*¹⁰.

The effect of chamfering the rearward-facing step was tested (Fig.10) but not that of rounding. At low speeds for the lower value of h^+ shown, there appears to be a substantial benefit in chamfering, but at the higher value of h^+ there appears to be a small penalty for a small amount of chamfer and there is little reduction in drag unless the chamfer angle is reduced to about 20 degrees. This result is confirmed by some measurements of Wieghardt². The drag increase does not occur at supersonic speeds but no substantial benefit is obtained unless the chamfer angle is reduced below 10 degrees.

For the drag of square ridges, mean lines only are shown in Fig.11. Also shown, as broken lines in the figure, are results for rectangular ridges of width $2h$, which were taken as a basic section to investigate the effects of rounding, since a limiting semicircular shape was thus obtained with $r = h$. As might be expected the drag of a ridge is closely related to the sum of the drags of forward- and rearward-facing steps. For square ridges at low speeds interference between the flows over the two faces leads to a drag parameter about 50% greater than the sum for the separate faces but the interference diminishes at supersonic speeds and is virtually zero at $M = 2.8$. Little published information has been found with which comparisons can be made. Again, the results at low speeds are in good agreement with Wieghardt², and the drag is slightly less than found by Good and Joubert⁵ for a fence. The results for rectangular ridges have lower slope than those for square ridges but have the same characteristic variation with Mach number.

The effects of rounding the top corners of the ridges are shown in Fig.12. It can be seen that at both subsonic and supersonic speeds there is an optimum in the radius for about $r = 0.6h$. The optimum is clearly defined at low speeds but becomes less pronounced at supersonic speeds. No previous information showing this detail has been found but the results for a semicircular ridge are again in close agreement with those of Wieghardt² (even in showing a non-linear variation with $\log h^+$, a feature not brought out in the presentation of Fig.12).

For sharp-edged steps and ridges, the drag may be estimated from the formula

$$\frac{C_D}{C_f} = C \log h^+ + D \quad (1)$$

where C and D have values as given below

	M	0.2	0.8	1.4	2.2	2.8
Forward	C	60	60	80	80	80
step	D	-80	-70	-65	-65	-65
Rear	C	16	20	48	50	35
step	D	-6	-13	-18	-30	-12
Square	C	150	150	160	110	100
ridge	D	-190	-160	-125	-42	-44

For grooves the drag increments were small and the accuracy of the measurements consequently poor. For grooves in the direction of the flow the drag increase measured by the balance was roughly equal to the local skin friction acting on the increased surface area, that is on the sides of the groove. For grooves normal to the flow a drag coefficient has been defined based on the surface area of the groove, and a Reynolds number based on the width of the groove l . Approximately the drag is given for all Mach numbers tested (0.2, 0.8, 1.4, 2.2, 2.8) and for three widths of groove ($l/h = 1, 2, 3$) with $h \approx 0.036$ by the formula

$$\frac{C_D}{C_f} = 2 \log \frac{u_\tau l}{\nu} - 2 \quad \text{for} \quad 10 < \frac{u_\tau l}{\nu} < 10^3 \quad (2)$$

The measurements are not sufficiently accurate to determine the effect of variation in l/h but the formula above is roughly consistent with the drag found for rectangular holes and shown in Figs. 16 and 17.

Except at very low Reynolds numbers the drag of a long groove normal to the flow is thus greater than that of the same groove along the flow. This result differs from that of Wieghardt² for screw slots. The difference is attributed to the drag of the ends of the slots being included in Wieghardt's measurements but not in those of the present work.

4.2 Circular holes

The flow pattern within a hole is of a complex three-dimensional nature and will depend upon the conditions of the flow approaching the hole and the geometry of the hole. It is unlikely that any simple analysis will be capable of describing all the possible flow patterns. For example for very shallow holes, reattachment of the flow leaving the forward edge will occur with subsequent further separation as the downstream edge is approached. In fact it

was found that for the shallowest holes tested a fair estimate of the drag could be made by assuming that the pressure variation on the vertical face of the hole was that of forward and rearward facing steps multiplied by the square of the cosine of the local angle of sweep of the edge of the hole. Within deeper holes complex vortex patterns will occur. However, in some way the flow within the hole will be driven by the shear stresses across the face of the hole and these shear stresses will be related to those in the boundary layer approaching the hole. An analysis has therefore been made by considering the drag of the hole as arising from an effective shear stress τ' , and this has been non-dimensionalised by the shear stress τ in the approaching boundary layer, so that an incremental drag parameter $C_D/c_f = \tau'/\tau - 1$ has been defined. Here C_D is the drag coefficient based on the planform area of the hole and c_f is the skin-friction coefficient of the approaching boundary layer. The drag parameter will depend upon a Reynolds number of the flow across the hole, taken as $u_\tau d/\nu$, where d is the hole diameter, on the Mach number of the flow, and on the hole depth to diameter ratio. Thus we may take

$$\frac{C_D}{c_f} = f\left(\frac{u_\tau d}{\nu}, \frac{h}{d}, M\right) \quad (3)$$

Inspection of the results for each hole and each Mach number over a range of Reynolds numbers showed that they could be expressed as

$$\frac{C_D}{c_f} = A \left(\frac{u_\tau d}{\nu}\right)^B, \quad (4)$$

where B was found to depend upon Mach number but was sensibly independent of hole depth whilst A depends strongly upon both Mach number and hole depth. Values of A and B are shown in Figs.13 and 14. There is practical interest in the drag of holes with depths greater than the maximum of $h/d = 1/3$ of the present tests. The results of previous work at low speeds have therefore been analysed in terms of equation (4). In making the analysis it has been necessary to estimate skin-friction coefficients and to assume that the value of B obtained from the present results could be taken even though the Reynolds numbers of the previous tests were lower. Values of A derived from the measurements of Wieghardt² agree with the present findings in the region of overlap and are shown in Fig.13. Consistent values have also been obtained from the tests of

Tillmann¹¹ and Friesing¹². These tests covered a wide range of values of d/δ , the ratio of hole diameter to boundary layer thickness, and the values of A show no strong dependency upon this parameter. The extension of the results to larger values of h/d reveals a strong almost periodic variation of A with h/d .

A brief oil-flow study has been made of the flow in holes in an attempt to find the flow patterns associated with this variation. The study was made in a small blower tunnel and it is not known if the drag variations implied by Fig.13 actually occur in the study. However, in view of the apparent generality of Fig.13 it is assumed that this is likely. The oil flow pattern for a hole of depth: diameter ratio, $h/d = 0.47$ was found to have a unique character compared with patterns for other holes in the range tested, $0.04 \leq h/d \leq 1.34$. A photograph of the pattern is given in Fig.15 in which linings to the floor and wall of the hole are shown. The photograph implies the existence of two vortex sheets, the upper one rolling up from a spiral point on the starboard wall, and presumably engulfing the lower sheet, emanating from the floor, in the rolling-up process. The coiled sheet appears to lie across the hole at about 45° to the stream direction, and its field appears to sweep new fluid into the hole roughly normal to its axis, as indicated by the streamlines on the floor. This powerful interchange of fluid presumably could account for the high drag but the reason for the formation of the pattern is not understood. It should be noted that though the pattern showed a preference for the asymmetry as shown in the photograph, patterns of the opposite hand occasionally occurred. Further details of the flow pattern for other values of the depth of the hole are given in the Appendix.

4.3 Rectangular holes

A few measurements have also been made with rectangular holes. Samples of the results are shown in Figs.16 and 17 at one Reynolds number only, $u_\tau \ell / \nu = 2 \times 10^4$, where ℓ is the length of the hole in the stream direction. Insufficient combinations of planform aspect ratio and depth to length ratio were tested to make any comprehensive analysis possible. In Fig.16 values of the drag parameter C_D/c_f are plotted against h/ℓ . The measurements show a trend of decreasing drag with increase of depth ratio. This trend is genuine for the three points with planform aspect ratio of 0.4 but may be coincidental for the points with aspect ratios of 1 and 2.5. As a check on this, results from Friesing¹² for holes with varying depth ratio are shown. These results are

at different Reynolds numbers and have simply been scaled so that the curves on Fig.16 pass through the points of the present measurements. The curves imply that the trend, whilst not being unique for different aspect ratios, is followed roughly. It is interesting to note that, if a 'lower bound' is fitted to the oscillatory curve of Fig.13 and the variation of the drag parameter on the lower bound for circular holes is then estimated at a mean Reynolds number of $\pi/4 u_d/v = 2 \times 10^4$, the general trend of the results for rectangular holes is well matched. This result suggests that at low speeds the drag of a circular hole which is not very shallow will generally exceed that of a rectangular hole of similar depth and streamwise extent.

In Fig.17 the variation of the drag of two particular holes with Mach number is shown and compared with the variation for a circular hole (of depth chosen so that the variation is not unduly influenced by the oscillatory characteristics). At subsonic speeds all three holes show an increase in drag with increase in Mach number, but at supersonic speeds the drag of the circular hole diminishes whilst the drag for the square and rectangular holes continues to rise. This trend is contrary to that found by McGregor¹³. Further work is needed to resolve the discrepancy and to put the estimation of the drag of rectangular holes on a firmer basis. McGregor's investigations concentrated on determining the effects of acoustic resonance on drag. The present results may be influenced by such effects but no positive evidence of their occurrence was found.

4.4 Circular cylinders

The flow past a circular cylinder normal to a wall is also very complex. At the base of the cylinder separation of the approaching flow leads to the formation of one or more horseshoe vortices wrapped round the front of the cylinder, and trailing in the downstream direction. If the flow is supersonic there will also be complicated shock patterns produced by the interaction of the bow shock of the cylinder and the boundary layer. Further out from the wall the variation of the drag along the cylinder will still not be simple since, even with the assumption that the drag may be treated stripwise, the local drag will depend upon the local values of kinetic pressure, Mach number, and Reynolds number. An attempt has been made in the analysis to take account of these various factors in an empirical way, ignoring of necessity the development of a proper model of the flow.

For cylinders which are very short compared with the boundary layer thickness, the drag is roughly the same as that of shallow holes, and can be estimated approximately in the same way by using the information on the drag of steps, with a factor for the angle of sweep of the vertical faces. This approach may be considered as a drag analogue to the law of the wall for a turbulent boundary layer. An extended analogy with velocity profiles has been considered for longer cylinders which project beyond the logarithmic region by introducing a drag defect function analogous to the usual velocity defect function as suggested by Good and Joubert⁵.

Measurements were made of the incremental drag created by cylinders of diameter $d = 12.7$ mm with length to diameter ratios s/d ranging from 1 to 20. The boundary layer thickness was of the order of $10d$. As a sample of the results the values of drag coefficient (based on frontal area) for a Mach number of 1.4 are shown in Fig.18 plotted against a Reynolds number Re_d based on freestream conditions and cylinder diameter. For all lengths of cylinder the drag increases with increase of Reynolds number but the rate of increase diminishes as the length of the cylinder increases.

In order to estimate the drag of cylinders which extend outside the boundary layer knowledge of the drag coefficient under freestream conditions, C_{D_∞} , is required. It has also been taken as a datum value on which to base other parts of the drag estimate. Its value has been found by extrapolation from results such as those in Fig.18 for the five Mach numbers at which measurements were made, and is shown in Fig.19, again plotted against Re_d . At $M = 0.2$ the range of Re_d extends just into the critical region, and it is of interest to note that the manner in which C_{D_∞} decreases falls within the band of previous measurements at low speeds, and that the critical value of Re_d is not exceptionally low as might have been anticipated from the effects of the proximity of the highly turbulent flow of the tunnel-wall boundary layer. At the other values of Mach number the separation over the rear of the cylinder is determined by compressibility effects and no drag decrease occurs with increase of Re_d . A further point to note is that the drag actually increases steadily with increase of Re_d ($dC_{D_\infty}/d \log Re_d$ being about 0.08). This increase is slower than that shown by Roshko¹⁴ for low speed flow at supercritical Reynolds numbers. The results of Fig.19 enable corrections for differences in Reynolds number to be made and a comparison with previous measurements to be obtained as shown in Fig.20.

The analogy with a velocity defect function is taken in the form

$$\frac{C_{D_\delta} - C_D}{c_f} = F\left(\frac{s}{\delta}\right) \quad (5)$$

where C_{D_δ} is the drag coefficient of a cylinder of length $s = \delta_{99}$ where δ_{99} is the boundary-layer thickness to 99% of freestream velocity. Within the range shown by the bars in Fig.21 it has been found that C_{D_δ} is proportional to C_{D_∞} at a given Mach number and the variation of the ratio is shown plotted against Mach number.

It had been hoped that a drag defect function independent of Mach number could be found, but for the reasons given previously the failure to find this, as shown in Fig.22, is not surprising.

Figs.20, 21 and 22 enable an estimate of drag to be made for cylinders of any length greater than about 0.1δ . For cylinders immersed completely in the boundary layer

$$C_D = C_{D_\delta} - Fc_f \quad (6)$$

and for cylinders which extend into the freestream

$$C_D = \frac{\delta}{s} C_{D_\delta} + \left(1 - \frac{\delta}{s}\right) C_{D_\infty} \quad (7)$$

The broken lines on Fig.18 show estimates derived from equations (6) and (7), with boundary-layer characteristics taken from Figs.1 and 2. The comparison with the measurements shows that the simplifications introduced in the estimation method lead only to small errors in the variation of drag with Reynolds number.

4.5 Stub wings

Four different stub wings were included, of spans 2.5, 1.25, 0.25 and $0.125c$, where c is the chord. The drag coefficient (based on frontal area) is shown plotted against Reynolds number based on chord in Fig.23. The results are similar in character to those for circular cylinders and it was hoped that the analysis made for the cylinders could be carried over to stub wings, or indeed to any other similar sort of object projecting into or through a boundary layer.

In particular it was hoped that the drag defect functions F (Fig.22) and the drag ratio (Fig.21) could be taken as being fairly universal so that given a knowledge of the drag of an object in the freestream its drag in a boundary layer could then be estimated. The drag of the stub wings at subsonic speed is small and has not been resolved with sufficient accuracy. Analysis has been made only of the results at supersonic speed. In the analysis the hopes are only partially realised. The drag defect function was found to have a variation both with Mach number and s/δ similar to that for circular cylinders but its values are scaled by a factor of $\frac{1}{2}$. However the drag ratio (Fig.25) whilst having values close to that for a circular cylinder at $M = 2.2$ and 2.8 was about 5% lower at $M = 1.4$. The drag coefficient of the wing section at free-stream conditions at supersonic speeds is shown in Fig.24. The streamlining of an aerofoil section compared with a circular cylinder gives a reduction in drag of some 40%. The estimates shown by the broken lines on Fig.23 are much less satisfactory than for circular cylinders.

4.6 Fairings

The measurements of the drag of fairings are the least satisfactory part of the investigation, and so far no general understanding of the results has been achieved but some observations can be made about them which give guide lines for design. The results, as drag coefficients based on the frontal area of the fairings, plotted against the ratio of boundary-layer thickness to fairing height are shown in Figs.26 and 27 for Mach numbers of 0.2 and 1.4 as being typical of the behaviour at subsonic and supersonic speeds respectively; sketches of the fairings are included with these figures. Altogether 10 configurations were tested, and the points shown are for the maximum and minimum Reynolds number for each configuration. There is some small inconsistency in the drag as presented because some of the excrescences extended beyond the front plate of the balance so covering parts of the wall the skin-friction drag of which was not included in the datum drag.

The first observation is that at subsonic speeds C_D increases with increased immersion of the fairings in the boundary layer and is considerably less than at supersonic speeds where the drag decreases with increased immersion. Apparently at subsonic speed viscous effects are dominant whereas at supersonic speed wave drag is diminished by the damping action of the boundary layer. This is shown most clearly by the results for the parabolic bodies (1), (2) and (3) of semi-circular cross-section and fineness ratio 3:1, for which an extended

range of δ/h was obtained by testing three sizes of body. At subsonic speed C_D tends to zero at infinite Reynolds number ($\delta/h = 0$), and at supersonic speed C_D has been extrapolated to an estimated value for the forebody drag plus a base drag. The estimate has been made in this way because it is known from observation of tufts that there was considerable separation over the rear of the body.

For the remaining bodies, which differ from bodies (1), (2) and (3) in having greater fineness ratio and in having end profiles of circular arc rather than parabolic arc form, the variation of drag with immersion in the boundary layer is greater. Body (8) which resembles (1), (2) and (3), but has a parallel mid-section, has a drag roughly consistent with that of these bodies, and with them has the lowest drag. Comparison of (8) with (4) and (5) (the arrows on the sketches of the bodies show the wind direction) indicates that a hemispherical forebody (body (5)) has a small penalty compared with a pointed body at subsonic speed and a large penalty at supersonic speed but that the reverse is true for a hemispherical afterbody (body (4)). Bodies (6) and (7) which have a rectangular cross-section of 2:1 aspect ratio have slightly higher drag than (8), which has a semi-circular cross-section. Their increased length compared with body (8) perhaps compensates for any improvement due to the increased fineness ratio of either the forebody or afterbody. The fact that their drag is roughly the same suggests that there is no advantage in increasing the forebody or afterbody length above a value of about $3h$. Finally the square cross-section bodies (9) and (10) have high drag but the variation with δ/h is rapid over the limited range investigated and comparison with other bodies might be different at different values of δ/h . The differences in drag between them confirms the penalties of a bluff afterbody at low speed and a bluff forebody at supersonic speed as indicated by the comparison of (4) and (5).

5 CONCLUDING REMARKS

It is suggested that the experimental results and the analysis given provide means of estimating the drag of many of the excrescences found on aircraft. There are, however, obvious shortcomings of the work, and considerable scope for extension on various aspects.

A notable omission is the lack of any study of effects which may accumulate downstream because of disturbances in the boundary layer and because of the effects of pressure gradients. Investigation is needed particularly of the downstream effects of three-dimensional forms of excrescence, and of the effects of

excrescences in three-dimensional boundary layers. The work of Nash and Bradshaw¹⁵ has shown that for simple excrescences in two-dimensional flow a 'magnification factor' to account for the effects of pressure gradients is calculable. Cook¹⁶ has given some further confirmation of this for the flow over an aerofoil with a ridge but has drawn attention to the powerful effects which may occur if the flow in the vicinity of the ridge is near critical. Further work is needed both on the drag of excrescences and on their overall effect on the flow over wings and bodies at transonic speed. The effect of sweepback on steps and ridges should also be studied.

The measurements of the drag of holes need extending to deeper holes, to holes with different planforms and cross-sections and exploration is needed of the possible benefits from shaping the edges of holes. Information is also needed on the drag caused by air intakes and outlets.

The investigation of the drag of fairings, though providing some guidance for the designer, is far from complete. The superficial assessment made so far, for example, covers, for the most part, only the effects of changes in Reynolds number on the total flow. More investigation is needed of the effects on drag of variation in size of the excrescence in relation to a given boundary-layer flow. Furthermore, since the purpose of fairings is to reduce the drag of some necessary obstacle, a proper approach, from purely aerodynamic considerations, would be to attempt to define a shape with minimum drag surrounding a given obstacle.

There are also other topics not covered in the investigation described here, amongst which are the increments in drag caused by surface distortions and by arrays of excrescences. To obtain a better understanding of the drag of arrays it is necessary to establish the way in which interferences between individual excrescences develop as their density increases and the drag changes from that for isolated excrescences to that for distributed roughness.

AppendixVISUALIZATION OF FLOW IN CIRCULAR CAVITIES

As noted in the main text an oil-flow study was made of the flow in circular cavities in low-speed airflow. Further details of the results of the flow visualization are described in this Appendix.

The observations were made in a blower tunnel with a working section 1.2m wide \times 0.3m high for cavities 146mm diameter and of varying depth, mounted in the floor of the tunnel. The turbulent boundary layer approaching the cavities was about 35mm thick and the tunnel speed was about 40 m/s. No measurements of forces on the cavities were made and it is assumed that the results of Fig.13 apply. The floor of the tunnel surrounding the holes and the walls and floors of the holes were lined with black plastics sheeting, on which the oil-flow patterns were formed and which were then removed for photographing. The oil-flows were obtained by brushing a mixture of oil and pigment over the surfaces. Because of the big variation in depth of holes there was a very wide range of surface shearing stress and no single mixture of oil and pigment was satisfactory. The oil was generally paraffin (kerosene) but for some configurations was mixed with a light machine oil or a light silicone oil. The pigment was either titanium dioxide or a 'Dayglo' powder. When the latter was used the photographs were taken under ultra-violet light.

The photographs, each with an attempted interpretation of the surface-streamline pattern in terms of the classical singularities described by Lighthill²², are shown in Figs.28 to 36. The presence of sharp edges and corners introduces features of the flow which are difficult to describe in these terms. In the figures the freestream flow direction is vertically down the page for the oil-flows of the floor of the tunnel and floor of the hole and also for the sketches of surface streamlines. The oil-flows on the walls of the holes are shown (except in Fig.28) with the surface unrolled, the cut in the walls being at the downstream centre-line of the holes and with the top edge of the hole uppermost. A certain amount of imagination has been used in drawing the streamline patterns, particularly for the deeper holes where the low shearing stresses allow the patterns to be dominated in places by oil running down the walls under gravity. A misleading indication of the flow along the plane of symmetry downstream of the holes is also given by the effects of oil accumulating on the downstream edge and washing away in bulk. The streamlines have also been treated in a fairly cavalier fashion at the sharp corners at the top and bottom of the

walls, and occasionally have been drawn as being continuous there, where in reality some local separations must occur. Such separations have been ignored where it has been considered that they have only a secondary influence on the overall flow pattern. In order to draw streamlines simply, without the complications of a proper perspective, the walls have been flattened to appear as an annulus between the floor of the hole and the floor of the tunnel, so that the whole surface is taken as planar. Though the patterns were accurately repeatable (apart from occasional switches of hand) some observations with smoke and tufts showed that the flow was extremely unsteady.

As noted in the main text the flow for a very shallow hole separates from the upstream edge, attaches on the floor, separates again on approaching the downstream edge and reattaches on the surface downstream of the hole. This type of flow is shown in Fig.28 where the hole depth: diameter ratio, h/d , is 0.04. The oil-flow for the wall of the hole is not shown in this figure. The main attachment on the floor of the hole is the nodal point N_1 , near the forward end. From this point part of the flow on the wall goes into two spiral points Sp_1 and Sp_2 which are also connected to two saddle points Sa_3 and Sa_4 . There is presumably also effectively a saddle point on the centre-line of the forward edge. At the aft end of the hole there are two saddle points Sa_1 and Sa_2 the latter of which is on the tunnel floor downstream of the hole. There will also be further complications beneath the streamlines from Sa_1 which enter the hole. The saddle points Sa_3 and Sa_4 are connected to the spiral points Sp_3 and Sp_4 . There also appear to be special features of the flow at the points P_1 and P_2 , where the edges of the hole are roughly streamwise. At these points the flow appears to divide, some flowing towards the saddle point Sa_1 and some streaming to downstream infinity. These points feature also in most of the remaining photographs and sketches.

The first peak in the drag of a hole (Fig.13) occurs at $h/d = 0.09$. The flow for this depth is shown in Fig.29, where it can be seen that the flow is reversed over most of the floor of the hole. The main attachment, Sa_1 of saddle type, occurs downstream of the hole and there is a complex arrangement of saddle points Sa_2, Sa_3, Sa_4, Sa_5 and spiral points Sp_1, Sp_2, Sp_3, Sp_4 over the upstream part of the floor, together with a further presumed saddle point on the forward edge. The flow is not quite symmetrical. Asymmetry appears to be a dominant feature of the behaviour of the flow and becomes more marked for moderate increase in depth. The asymmetry is not thought to be caused by asymmetry in the approach flow since flows of either hand could occur, and the

flow could be seen to change hand when the flow in the tunnel was deliberately disturbed in an appropriate way.

It might be argued speculatively that, as the boundary layer approaching the hole leaves the curved edge of the hole, there will be a progressive change in the mean speed in the layer so that the transverse vortex vectors will be turned, leading to the creation of streamwise vorticity. This vorticity will be of opposite sign on the two sides of the hole. Any chance disturbance will lead to the vorticity on one side or the other becoming larger and the vorticity of larger magnitude may then reinforce the mechanism which created it and so dominate the flow.

In Fig.30 h/d is increased to 0.29. This is at a trough in the drag. The flow is now markedly asymmetrical. There are three spiral points within the hole, one on the floor, Sp_2 , and two, Sp_1 and Sp_3 , on the wall. The two spiral points on the wall appear to be joined by a separation line within the hole originating from a saddle point Sa_2 so that in a sense the flow is contained. It is assumed that the low drag of this hole is associated with this containment which implies that there is not a great exchange of fluid between the hole and the outer flow. The saddle point Sa_2 appears to be fed by flow coming down the wall from the sharp edge.

However, when the depth is further increased to $h/d = 0.47$ (Fig.31) which is the depth ratio for the highest drag, one of the spiral points (Sp_1 in the previous figure) in effect lifts clear of the hole so that there is the opportunity for considerable spillage. The saddle point, Sa_2 , which joined the two wall spirals for $h/d = 0.29$ has now moved on to the flat surface downstream of the hole at the left-hand side. From this saddle point there appears to be a streamline going 'upstream' along the edge of the hole and finally entering the hole. Alongside this streamline flow appears to be emerging vertically from the hole under the influence of the strong circulatory motion within the hole. On the right-hand side of the downstream part of the wall there is a combination of nodal (N_1) and saddle (Sa_1) attachment points.

As the depth of the hole is increased to $h/d = 0.60$ (Fig.32) the free end of the vortex lying across the hole moves down into the hole and becomes joined to the left-hand wall once more at Sp_1 . This presumably reduces the spillage of air from the hole and the drag falls. The complicated combination of nodal (N_1) and saddle (Sa_1) attachment points on the downstream wall remains and there appears to be an additional point Sa_4 on the downstream edge.

At a depth $h/d = 0.78$ (Fig.33) this complication has disappeared and the flow is virtually the same as at $h/d = 0.29$. The drag is low as it also is for $h/d = 0.29$.

The final three sets of figures, 34, 35, 36 are at $h/d = 0.86, 1.07, 1.34$. The flows appear to be all of the same kind and to be much more nearly symmetrical than for smaller depths of hole, the single spiral point on the floor being replaced by a pair (Sp_2 and Sp_4). Over this range of depths the drag varies by a factor of more than 2:1. It does not seem possible, on the basis only of surface oil-flows, to give a clear reason for this drag variation. However, it might be noted that the 'wake' for $h/d = 1.07$ appears to be wider than for $h/d = 0.86$ and 1.34. Since qualitatively the three flows appear the same, the drag variation is presumably associated with a quantitative change. Further understanding will probably therefore only be obtained by detailed pressure plotting.

SYMBOLS

A } B }	constants in expression for drag of circular holes (equation (4))
C } D }	constants in expression for drag of steps and ridges (equation (1))
c	chord of stub wing
C_D	drag coefficient based on either frontal or plan area and freestream kinetic pressure
C_{D_∞}	drag coefficient of circular cylinder or stub wing of infinite length
C_{D_δ}	drag coefficient of circular cylinder or stub wing of length $s = \delta_{99}$
c_f	local skin-friction coefficient in absence of excrescence
d	diameter of circular hole or circular cylinder
F	drag defect function (equation (5))
h	height of step, height of body or depth of hole
$h^+ = u_\tau h/\nu$	
l	streamwise length of rectangular hole, length of chamfer of step, or width of groove
M	Mach number
r	radius of rounding of step or ridge
Re_c	Reynolds number based on freestream conditions and chord c of stub wing
Re_d	Reynolds number based on freestream conditions and diameter d of circular cylinder
s	span of stub wing or circular cylinder
w	width of rectangular hole
δ	loosely, boundary layer thickness or specifically thickness to 99% free-stream velocity (δ_{99})
ν	kinematic viscosity based on wall conditions
ρ	density at wall conditions
τ	surface shearing stress
τ'	effective shearing stress on a hole
u_τ	friction velocity based on wall conditions = $(\tau/\rho)^{1/2}$

REFERENCES

- | <u>No.</u> | <u>Author</u> | <u>Title, etc.</u> |
|------------|--|---|
| 1 | A.B. Haines | Subsonic aircraft drag: an appreciation of present standards.
Aeronaut. J. Vol. 72, No. 687, pp 253-266, March 1968 |
| 2 | K. Wieghardt | Increase of the turbulent frictional resistance caused by surface irregularities.
MAP R & T No. 103, June 1946 (Translation of ZWB FB 1563, 1942) |
| 3 | S.F. Hoerner | Fluid-dynamic drag (1965) |
| 4 | K.G. Winter
L. Gaudet | Turbulent boundary-layer studies at high Reynolds numbers at Mach numbers between 0.2 and 2.8.
R & M 3712, December 1970 |
| 5 | M.C. Good
P.N. Joubert | The form drag of two-dimensional bluff-plates immersed in turbulent boundary layers.
J. Fluid Mech., Vol. 31, Part 3, pp 547-582 (1968) |
| 6 | C.E. Kepler
S.M. Bogdonoff | Interaction of a turbulent boundary layer with a step at $M = 3$.
Princeton Aero Eng Rep 238, September 1953 |
| 7 | I.E. Vas
S.M. Bogdonoff | Interaction of a turbulent boundary layer with a step at $M = 3.85$.
Princeton Aero Eng Rep 295, April 1955 |
| 8 | K.R. Czarnecki
J.R. Sevier
M.M. Carmel | Effect of fabrication-type roughness on turbulent skin friction at supersonic speeds.
NACA TN 4299, July 1958 |
| 9 | R.C. Hastings | Turbulent flow past two-dimensional bases in supersonic streams.
R & M 3401 (1963) |
| 10 | I. Tani
M. Inchi
H. Komoda | Experimental investigation of flow separation associated with a step or a groove.
Aero Res. Inst. Univ of Tokyo Rep 364, April 1961 |
| 11 | W. Tillmann | Additional measurements of the drag of surface irregularities in a turbulent boundary layer.
NACA TM 1299, January 1951 (Translation of ZWB UM 6619, 1944) |

REFERENCES (continued)

- | <u>No.</u> | <u>Author</u> | <u>Title, etc.</u> |
|------------|----------------------------|--|
| 12 | H. Friesing | Measurement of the drag associated with recessed surfaces: cut-outs of rectangular and elliptic planform.
RAE Library Trans. 1614, October 1971
(Translation of ZWB FB 628 1936) |
| 13 | O.W. McGregor | Aerodynamic drag of two-dimensional rectangular notches in transonic and supersonic turbulent flow (with emphasis on the effects of self-induced pressure oscillations).
Illinois Univ.Ph.D.Thesis (1969) |
| 14 | A. Roshko | Experiments on the flow past a circular cylinder at very high Reynolds number.
J. Fluid Mech., Vol.10, pp 345-356 (1961) |
| 15 | J.F. Nash
P. Bradshaw | The magnification of roughness drag by pressure gradients.
J. R. Aeronaut.Soc., Vol.71, pp 44-49, January 1967 |
| 16 | T.A. Cook | The effects of ridge excrescences and trailing-edge control gaps on two-dimensional aerofoil characteristics.
R & M No.3698, April 1971 |
| 17 | C.J. Welsh | The drag of finite-length cylinders determined from flight tests at high Reynolds numbers for a Mach number range from 0.5 to 1.3.
NACA TN 2941, June 1953 |
| 18 | T.E. Stanton | On the effect of air compression on drag and pressure distribution of cylinders of infinite aspect ratio.
R & M 1210 (1929) |
| 19 | F.E. Gowen
E.W. Perkins | Drag of circular cylinders for a wide range of Reynolds numbers and Mach numbers.
NACA TN 2960 (1953) |
| 20 | D.M. Sykes | The supersonic and low-speed flows past circular cylinders of finite length supported at one end.
J. Fluid Mech., Vol.12, pp 367-387 (1962) |

REFERENCES (concluded)

<u>No.</u>	<u>Author</u>	<u>Title, etc.</u>
21	L.W. Walter A.H. Lange	Surface temperature and pressure distributions on a circular cylinder in supersonic cross-flow. NAVCORP Rep 2854, June 1953
22	L. Rosenhead (Ed.)	Laminar boundary layers. Clarendon Press (1963)

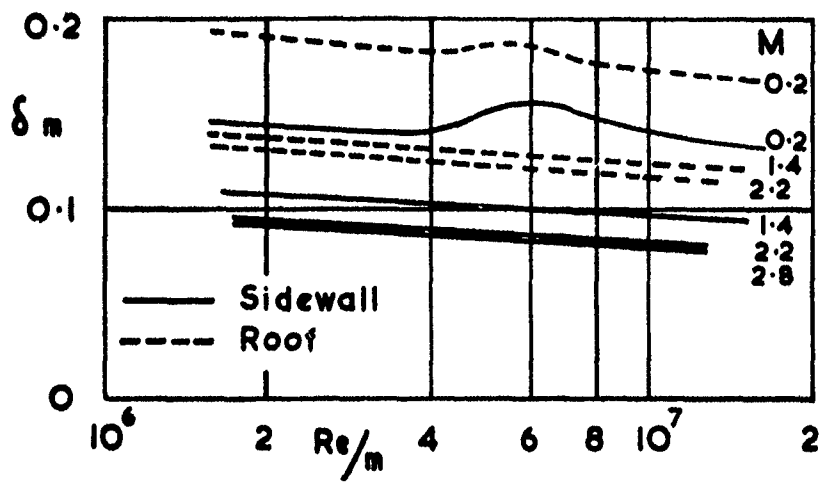


Fig. 1 Boundary-layer thickness

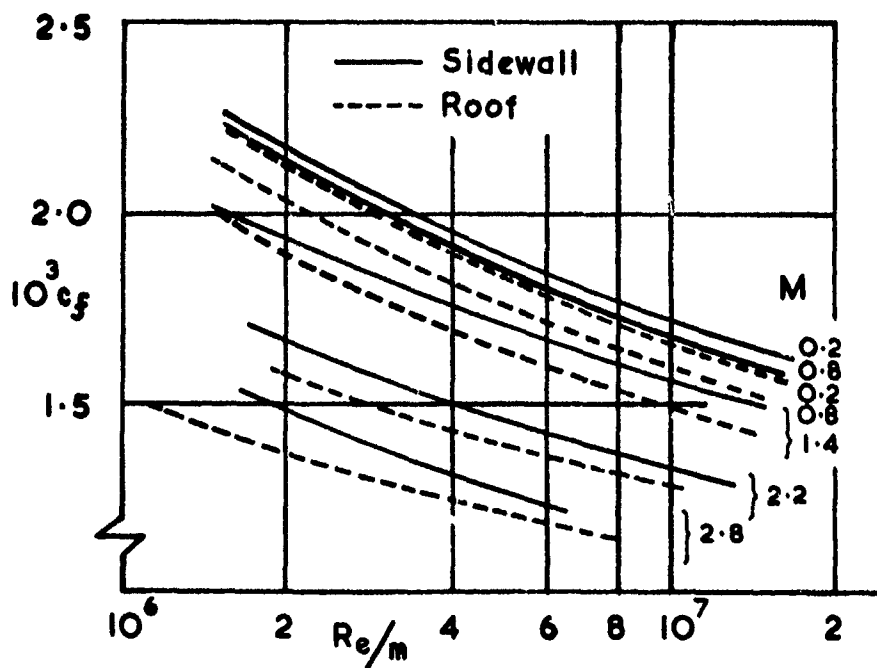


Fig. 2 Skin-friction coefficient

Fig.3

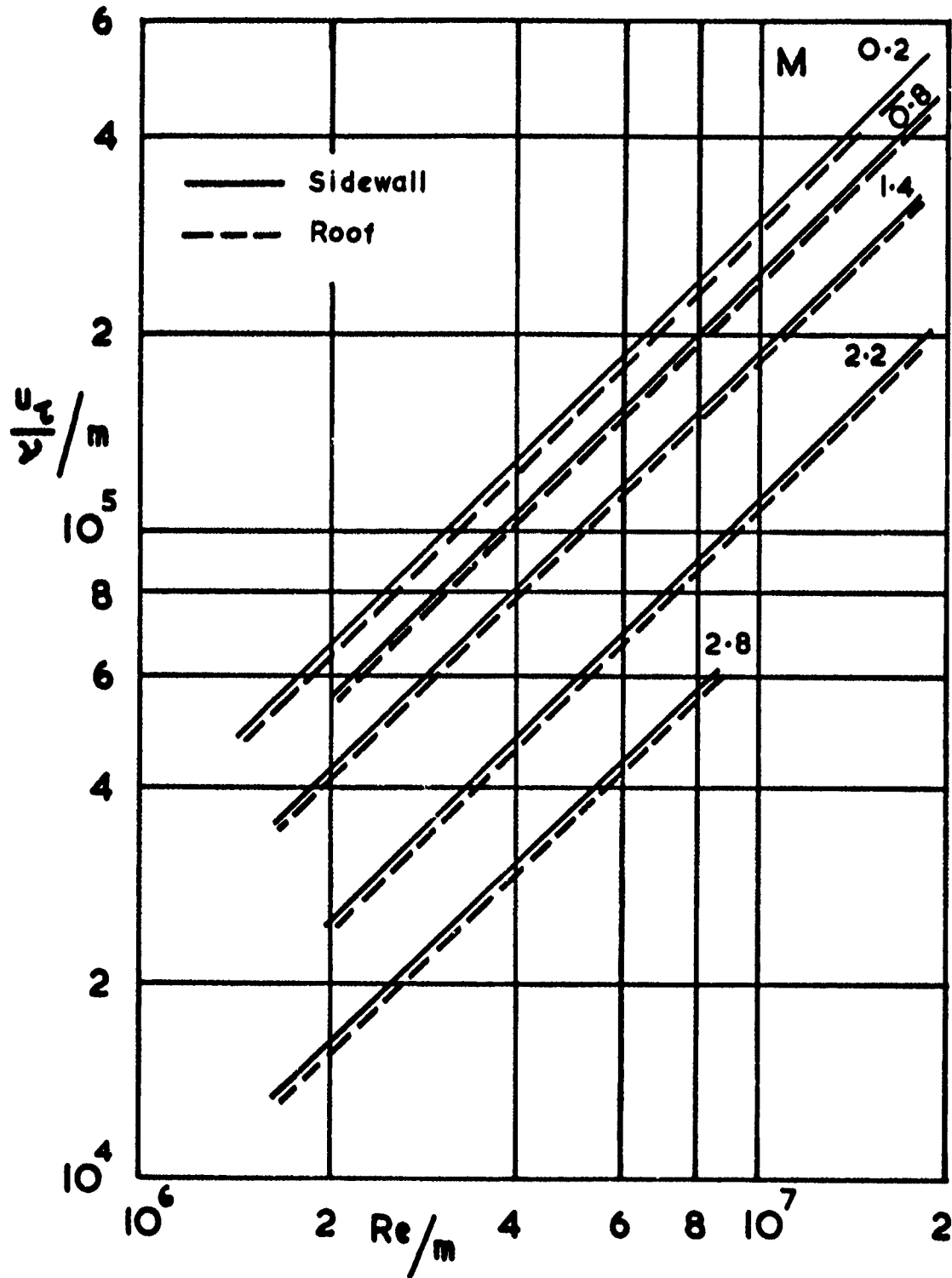
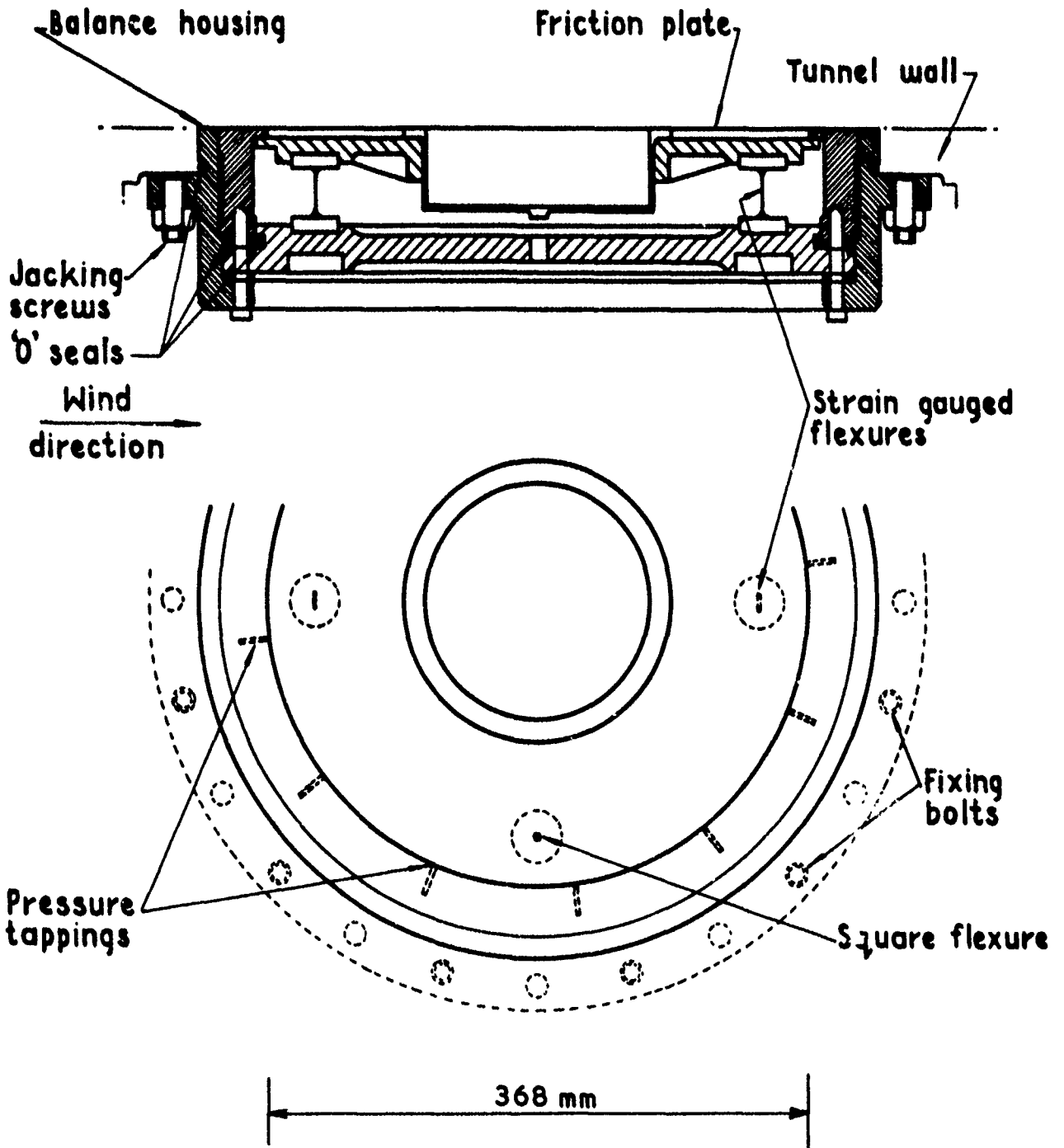


Fig.3 Friction Reynolds number

Fig.4



T. Memo Aero 1538

Fig.4 Details of balance (with circular hole)

Fig.5



Fig.5 Fairings for use with steps

Fig. 6-8

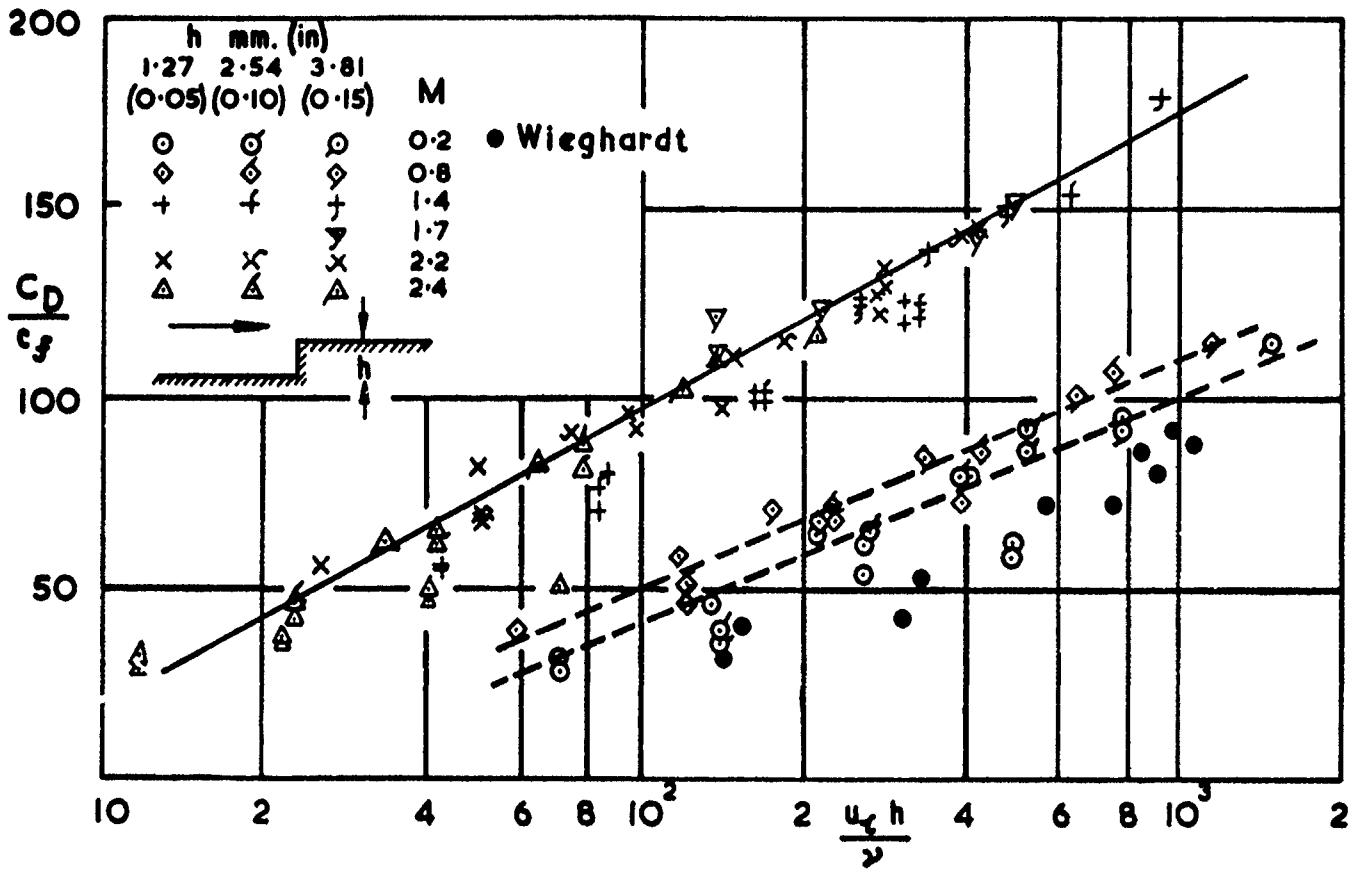


Fig. 6 Forward-facing steps - plain

T. Memo Aero 1538

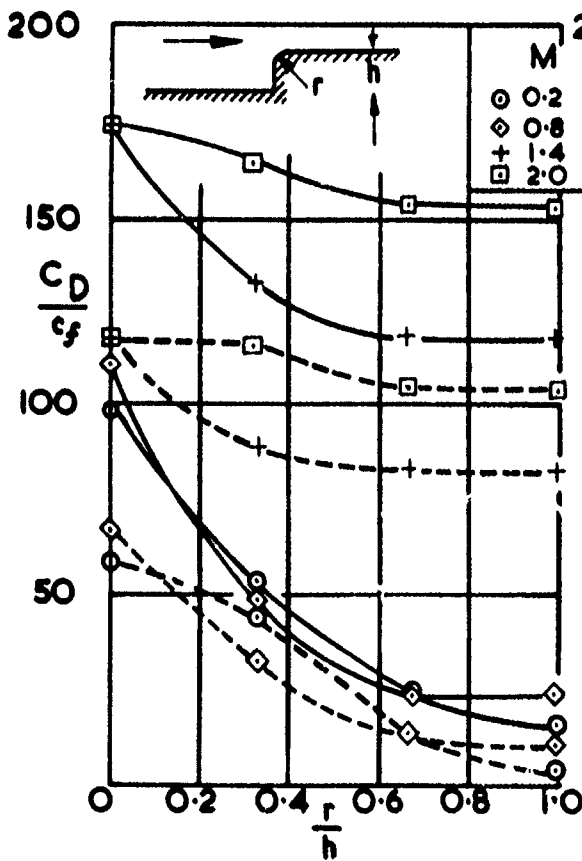


Fig. 7 Forward-facing steps effect of rounding

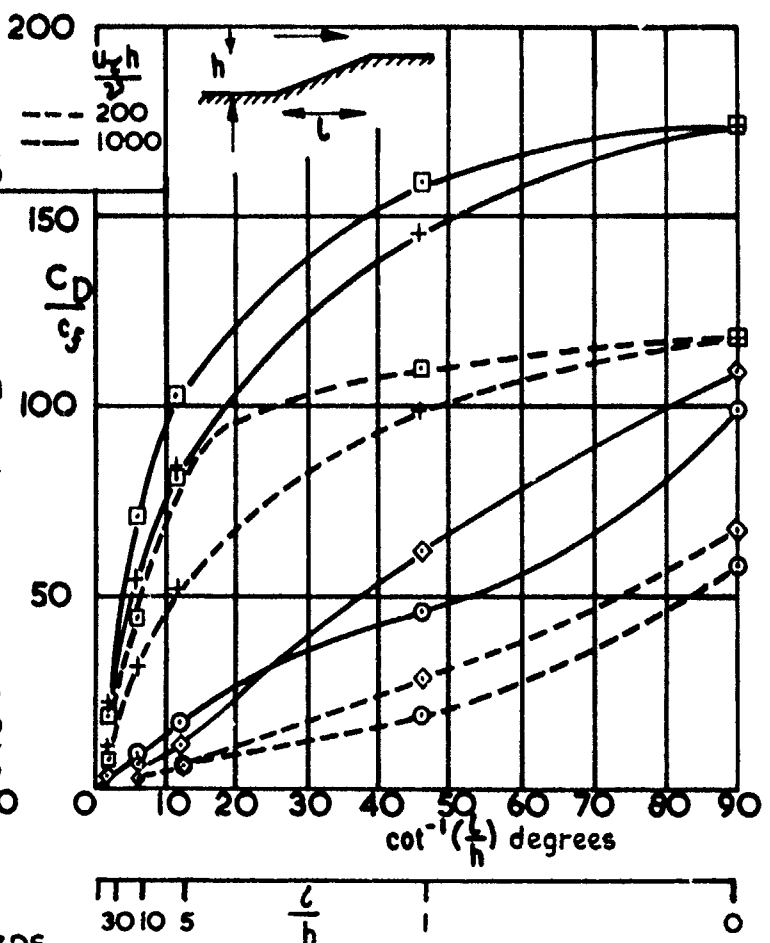


Fig. 8 Forward-facing steps - effect of step length

Fig. 9 & 10

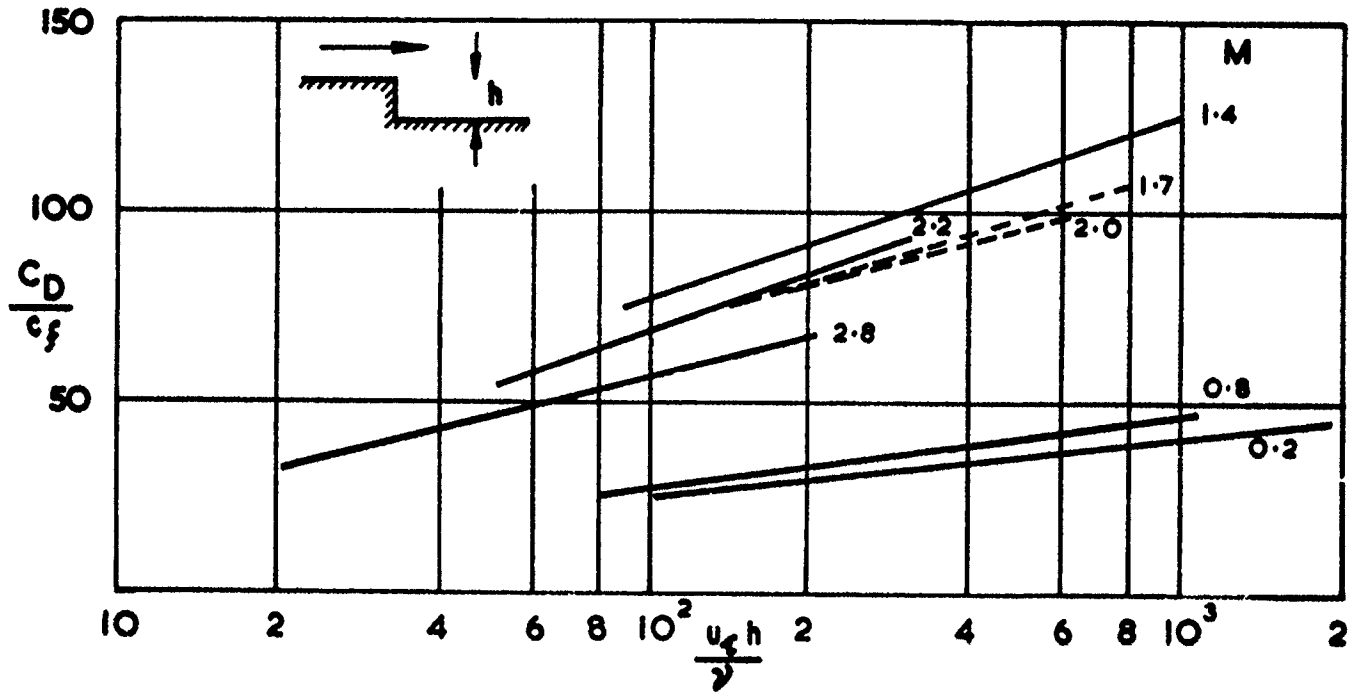


Fig. 9 Rearward-facing steps - plain

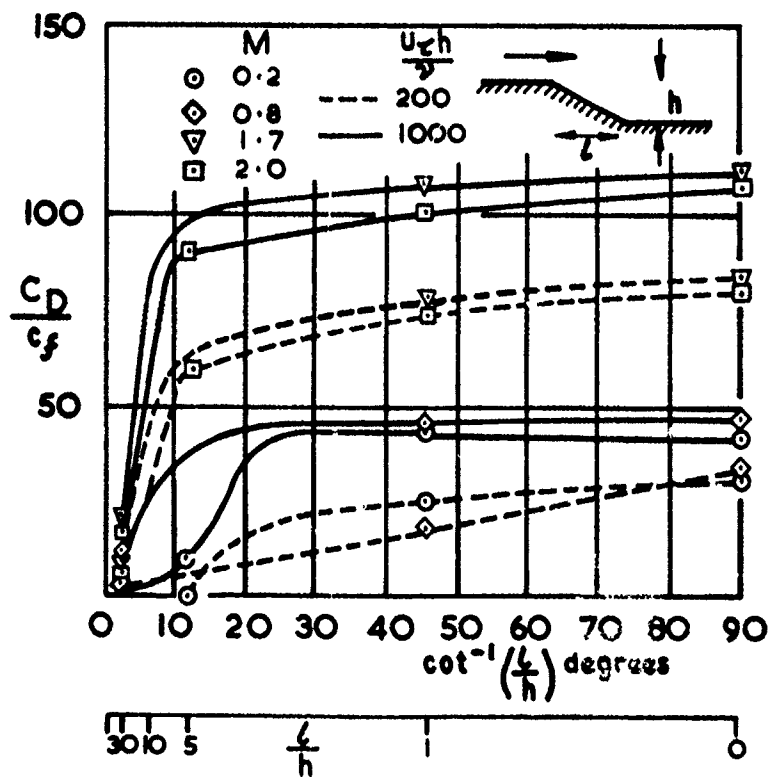


Fig.11 & 12

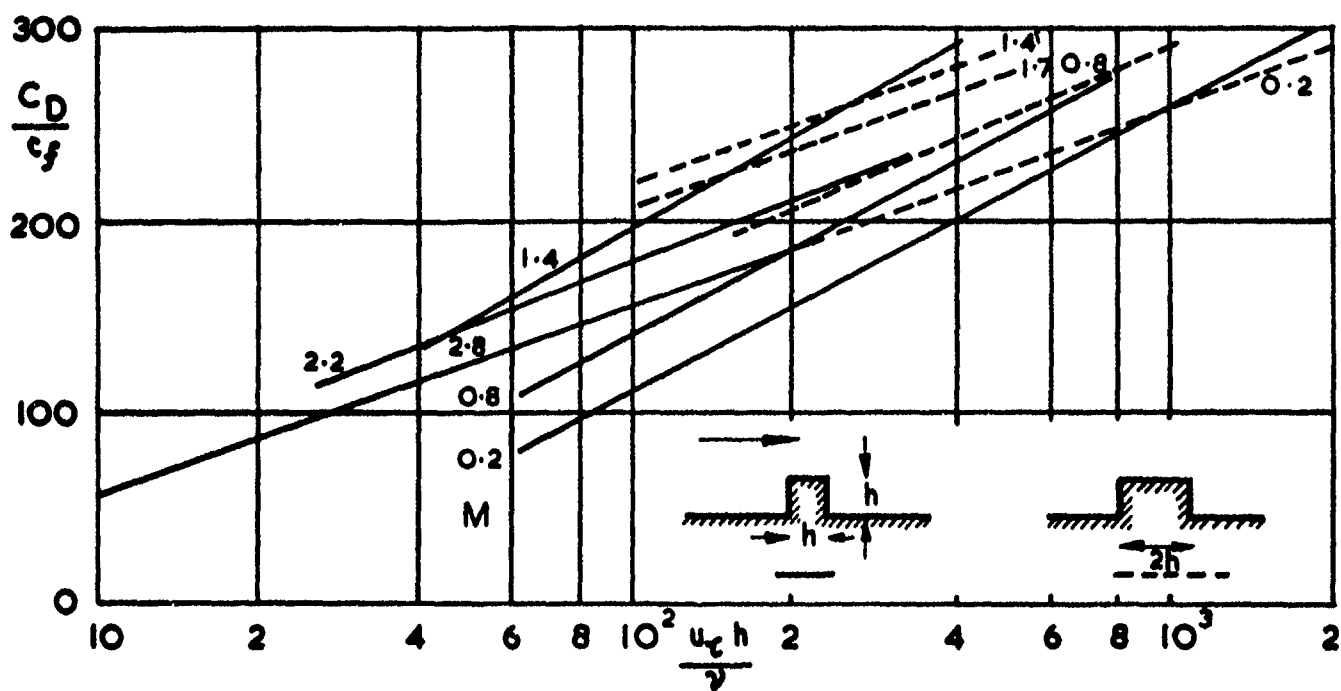


Fig.11 Plain ridges

T Memo Aero 1538

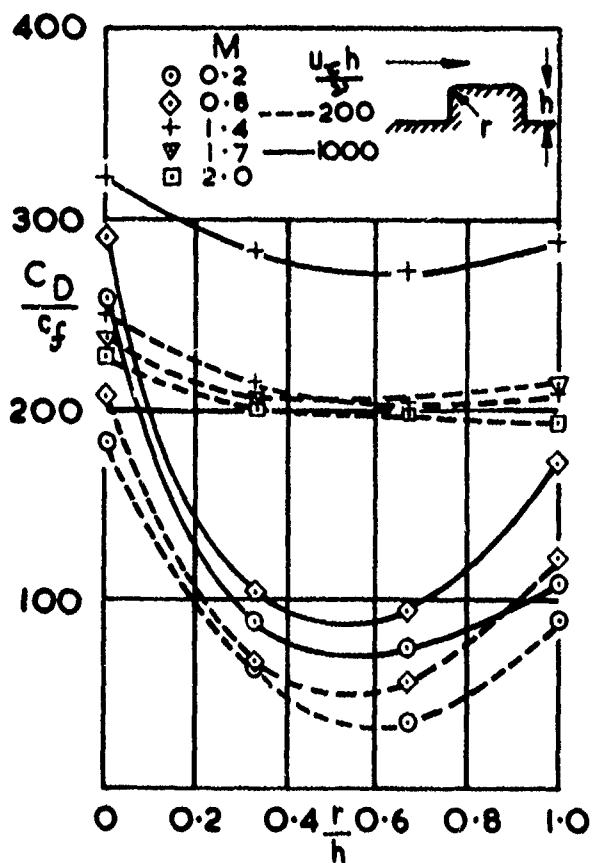


Fig.12 Ridges - effect of rounding

Fig.13&14

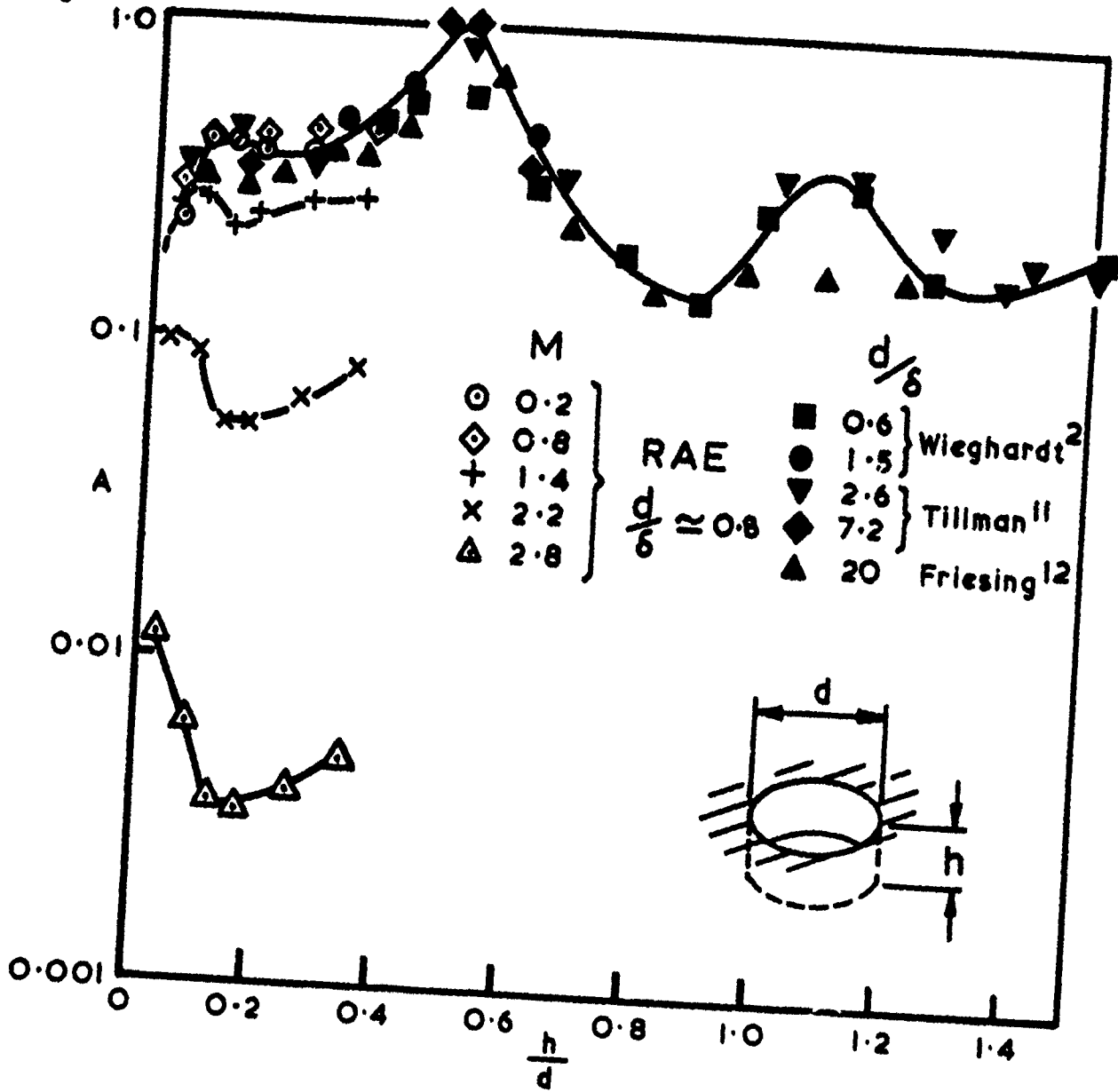


Fig.13 Variation of A with M & $\frac{h}{d}$

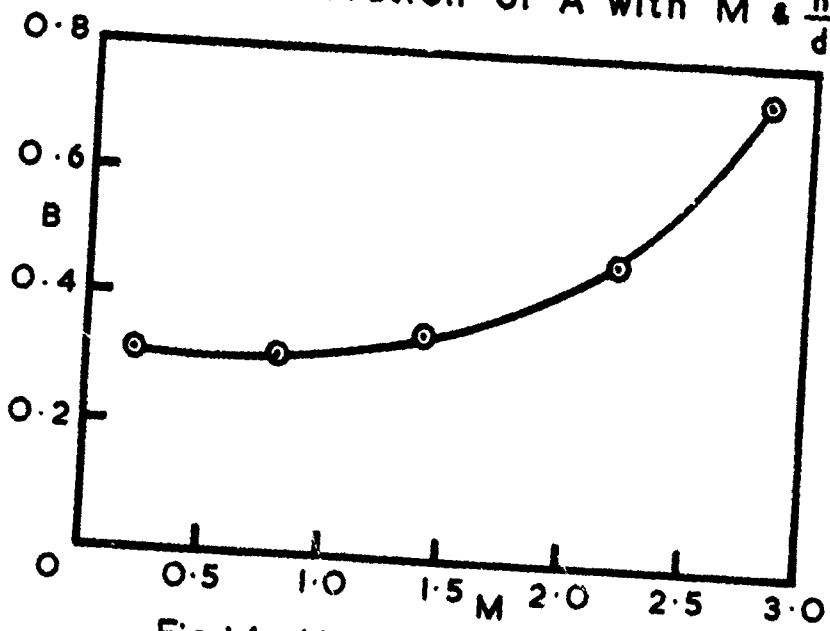


Fig.14 Variation of B with M

$C_D = \frac{1}{2} \rho u_\infty^2 B$

Fig.15

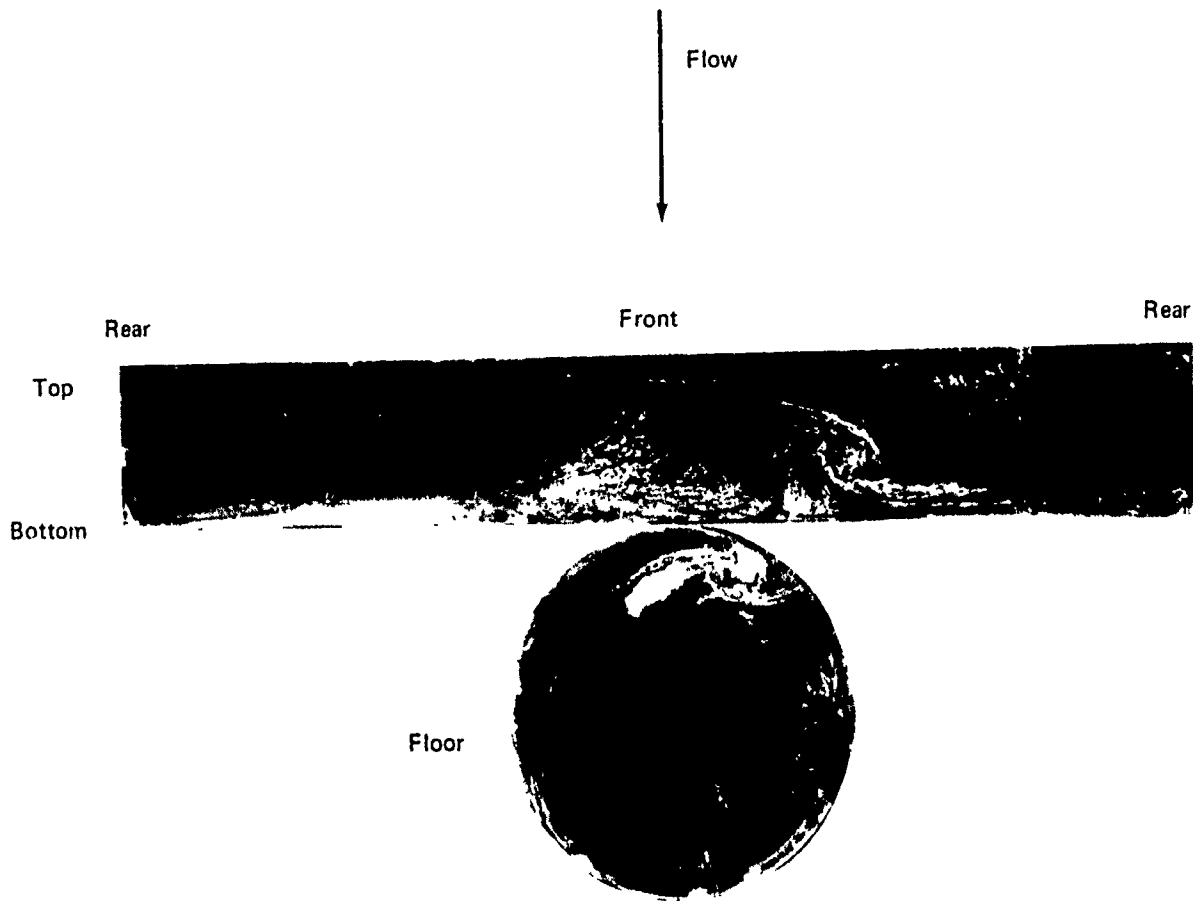


Fig.15 Oil-flow pattern in circular hole $\frac{h}{d} = 0.47$

Fig.16 & 17

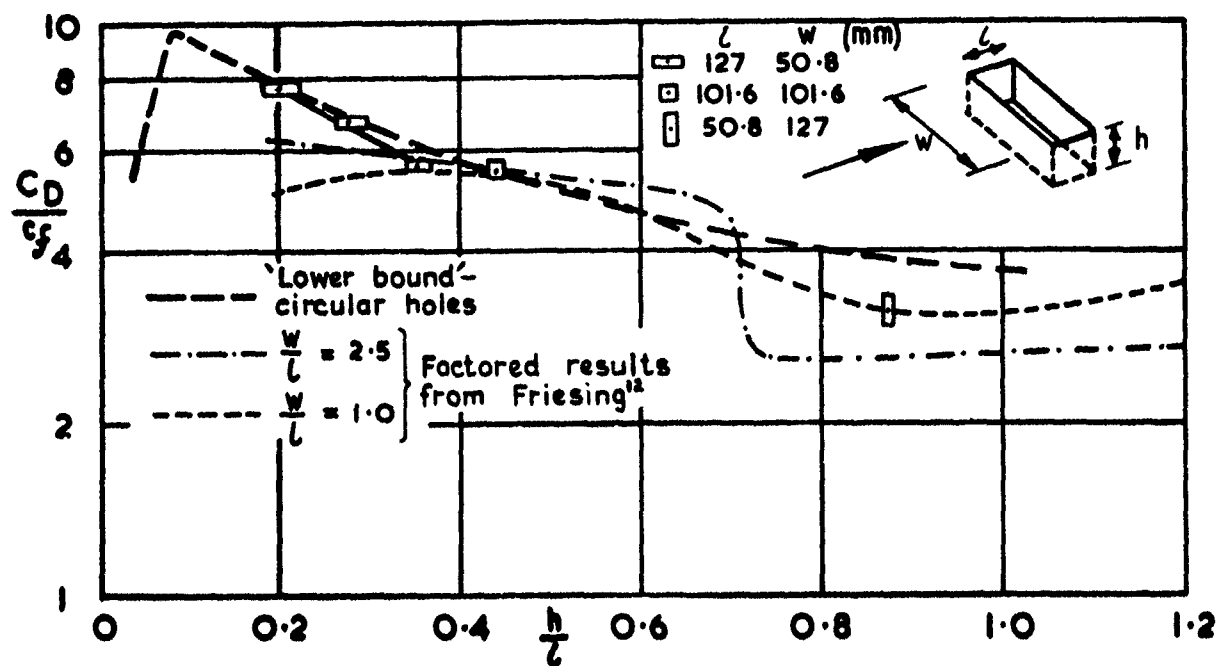


Fig.16 Rectangular holes $M=0.2$ $\frac{u_{\infty} l}{\nu} = 2 \times 10^4$

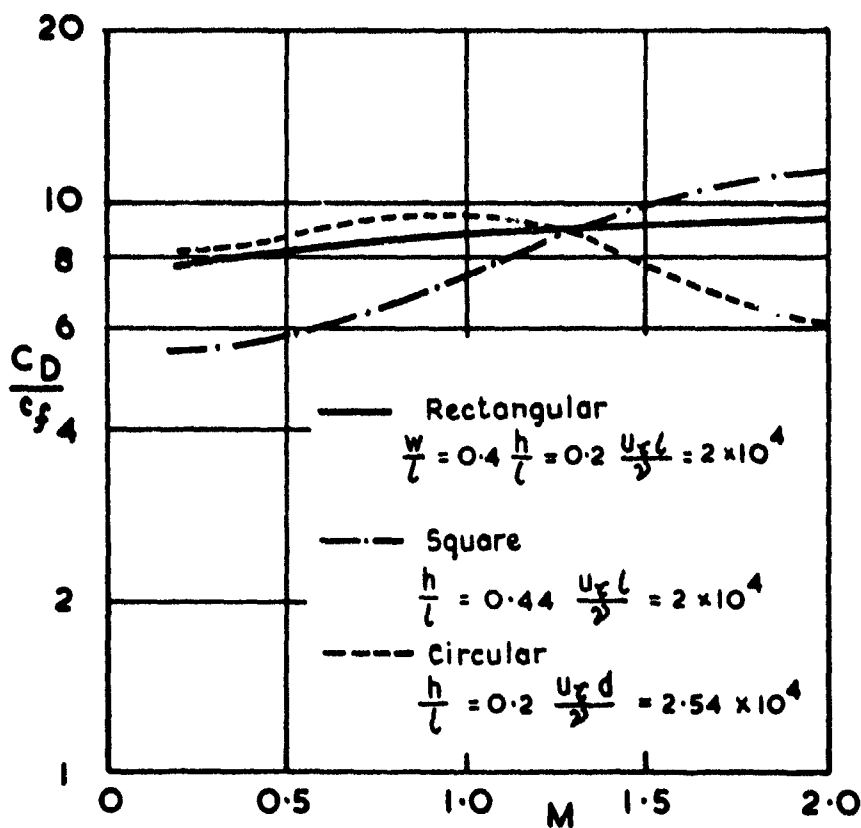


Fig.17 Rectangular holes - variation of drag with Mach number

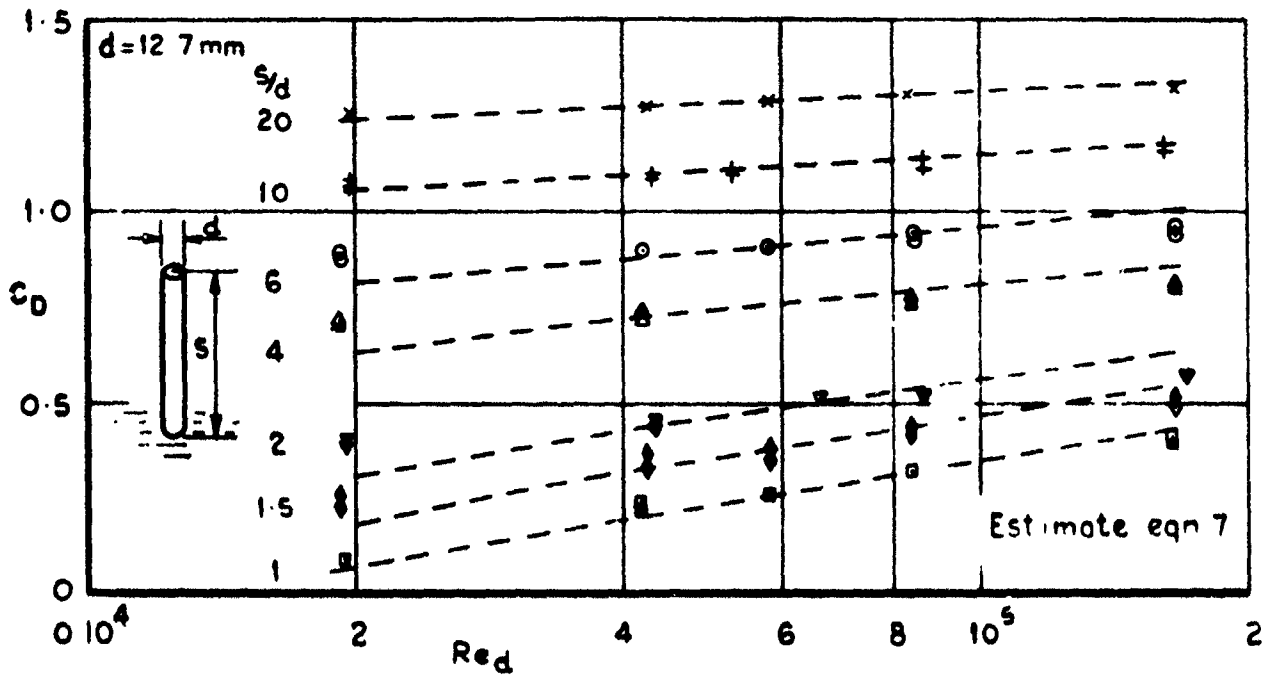


Fig.18 Drag of circular cylinders—typical results $M=1.4$

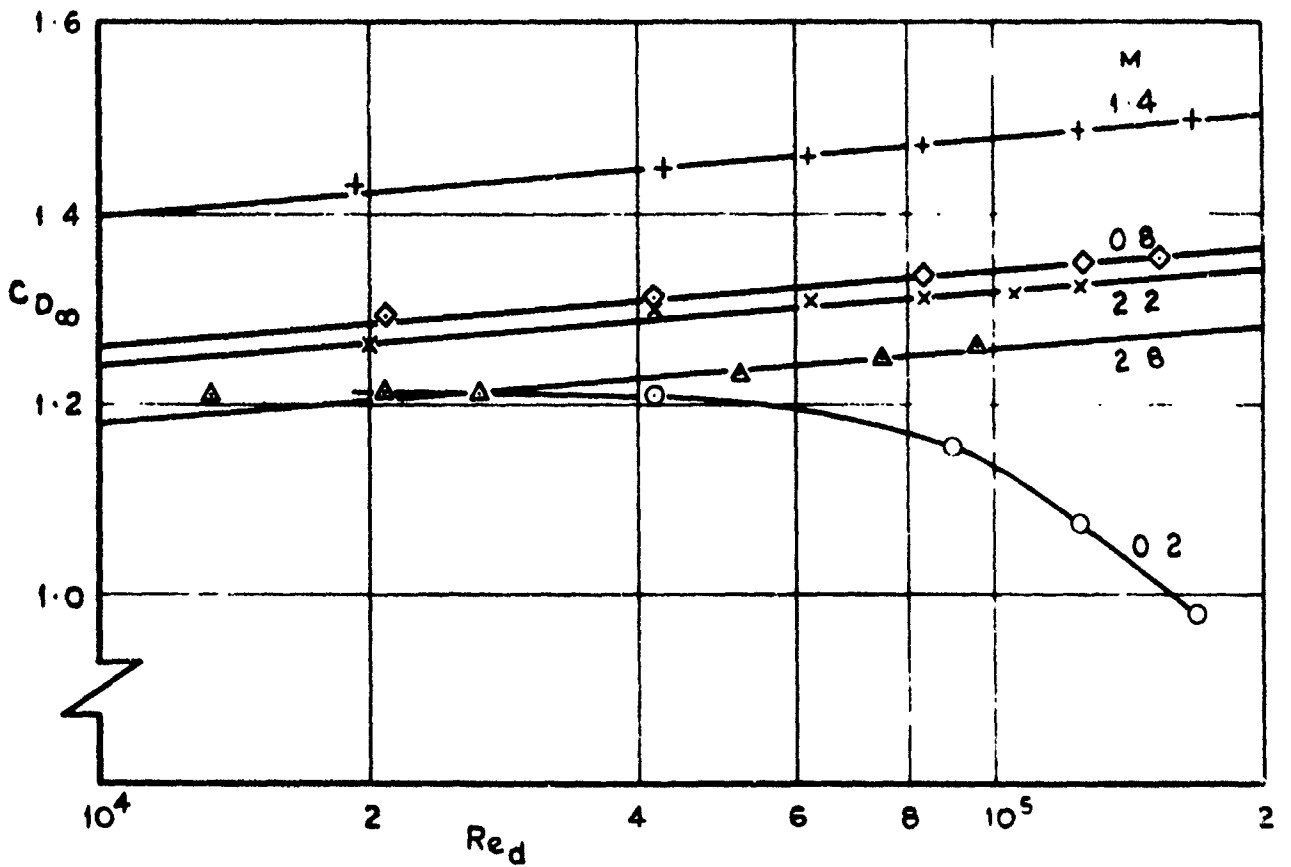


Fig.19 Drag of cylinders of infinite length

1 PIERO AERO 1538

Fig. 20 & 21

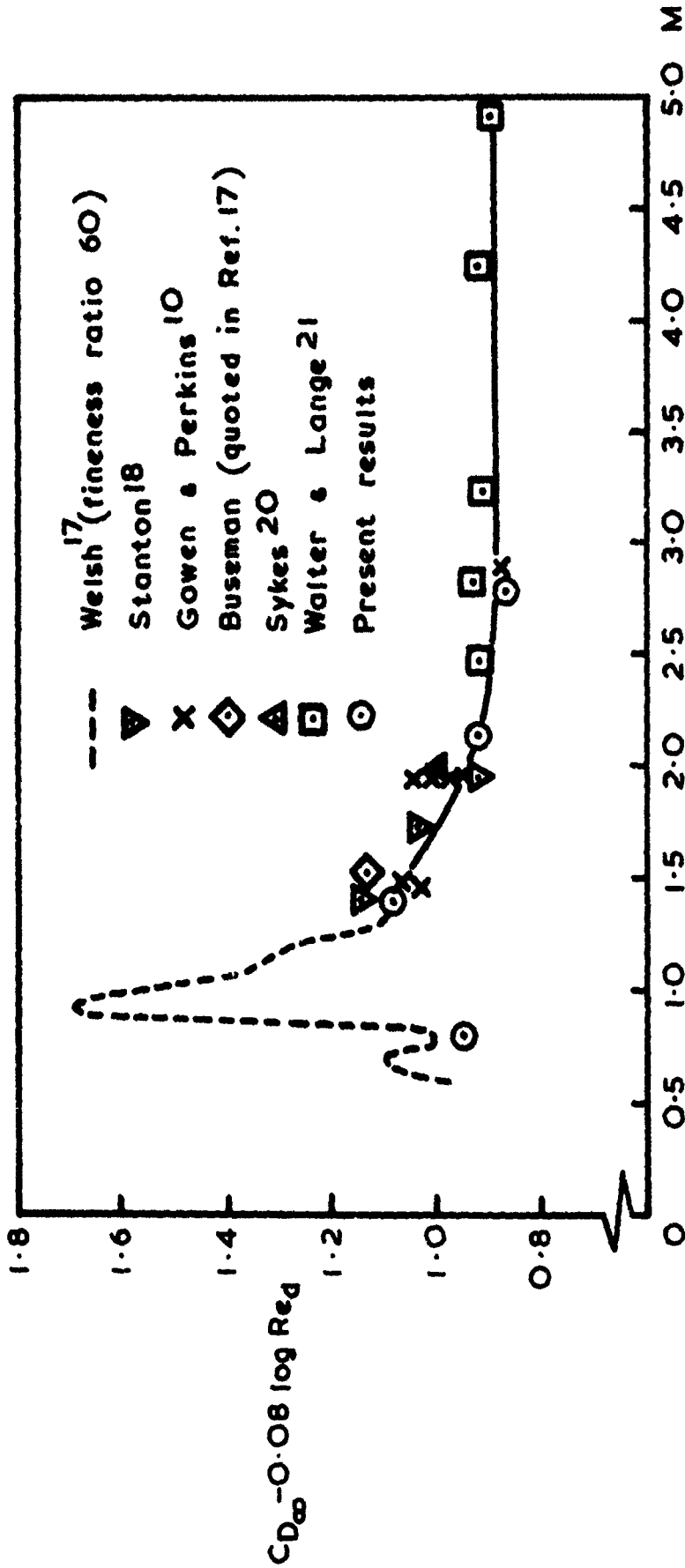


Fig. 20 Drag of cylinders of infinite length

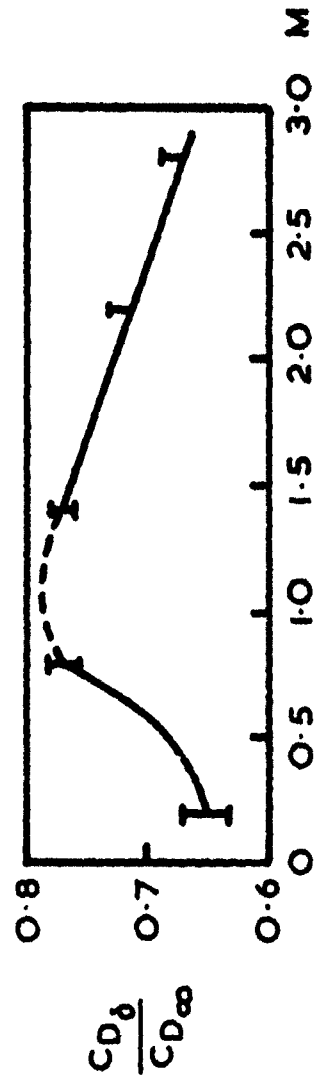


Fig. 21 Drag of cylinder of length $s = 0.99$

T. Memo Aero 1538

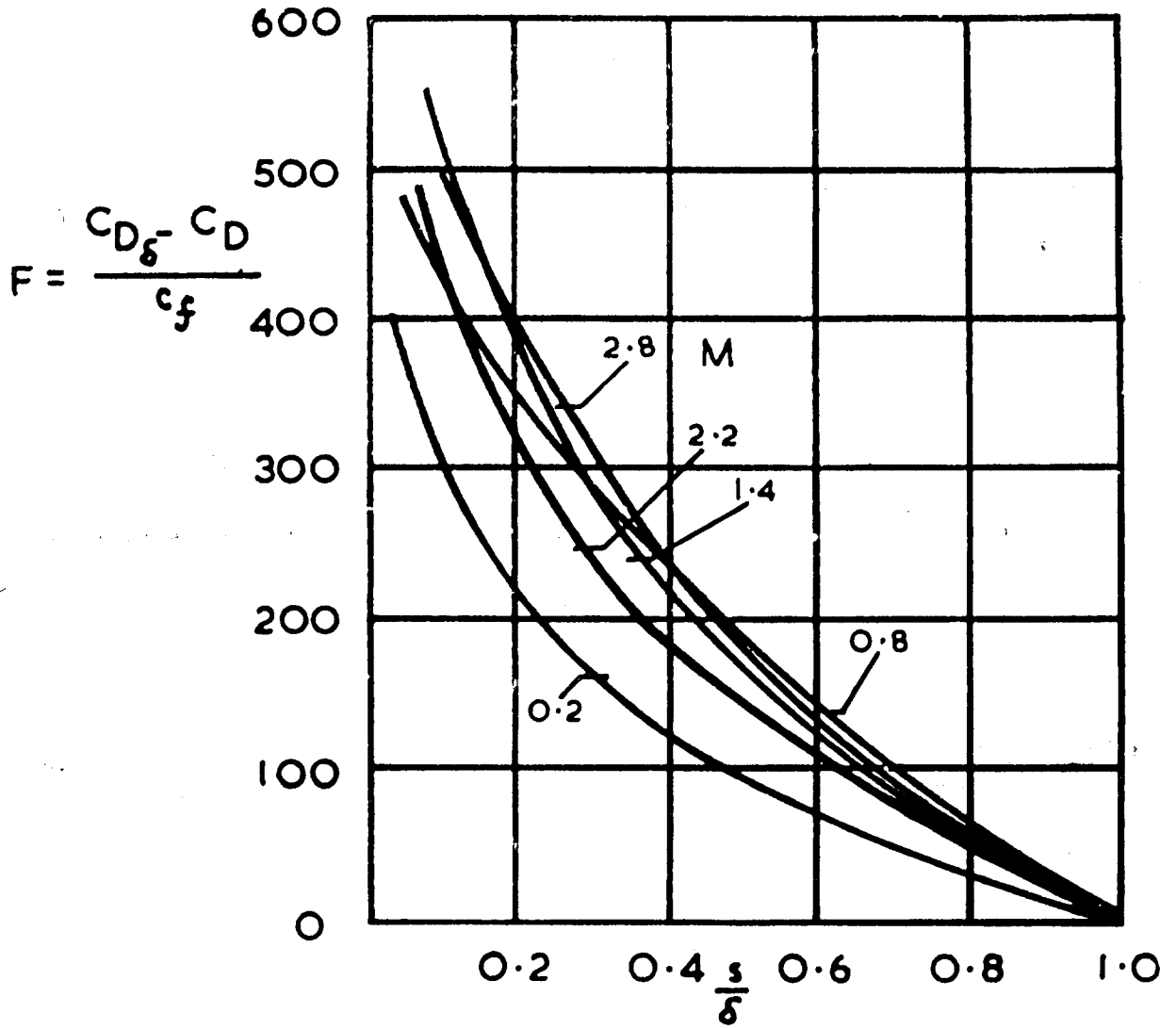


Fig.22 Circular cylinders - drag defect function

Fig. 23 -25

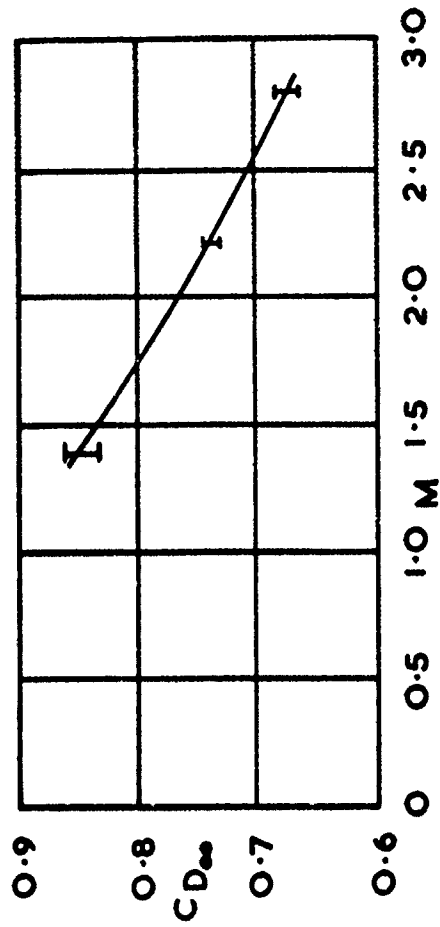


Fig. 24 Drag of wing section in freestream

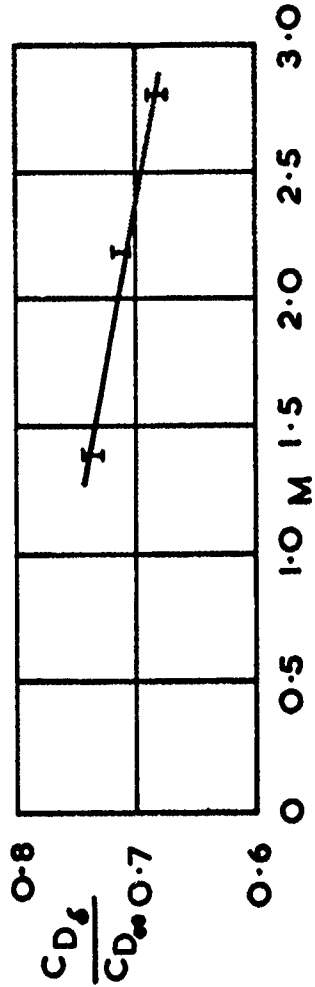


Fig. 25 Drag ratio for $s = \delta_{99}$

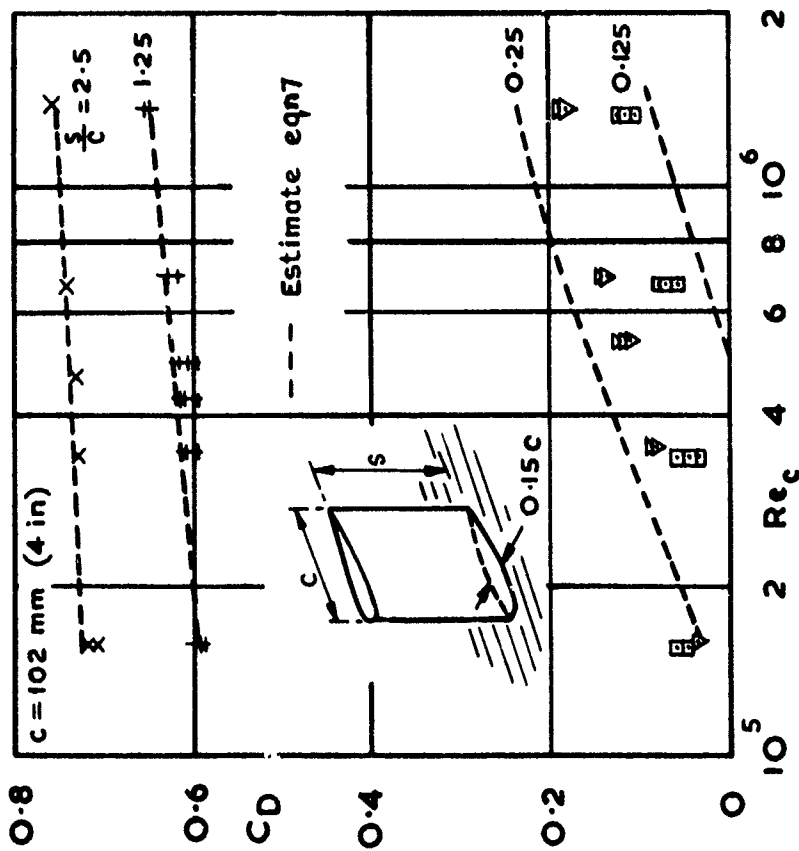


Fig. 23 Drag of stub wings - typical results $M = 1.4$

Fig.26 & 27

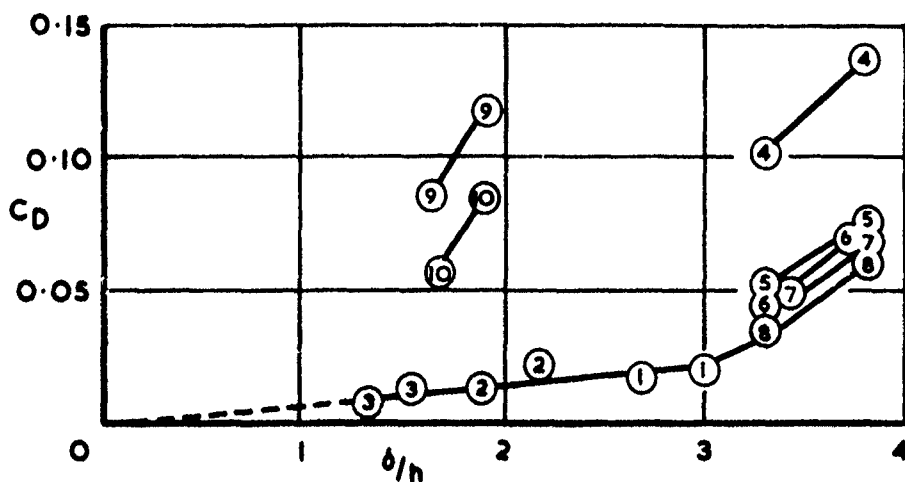


Fig.26 Fairings M=0.2

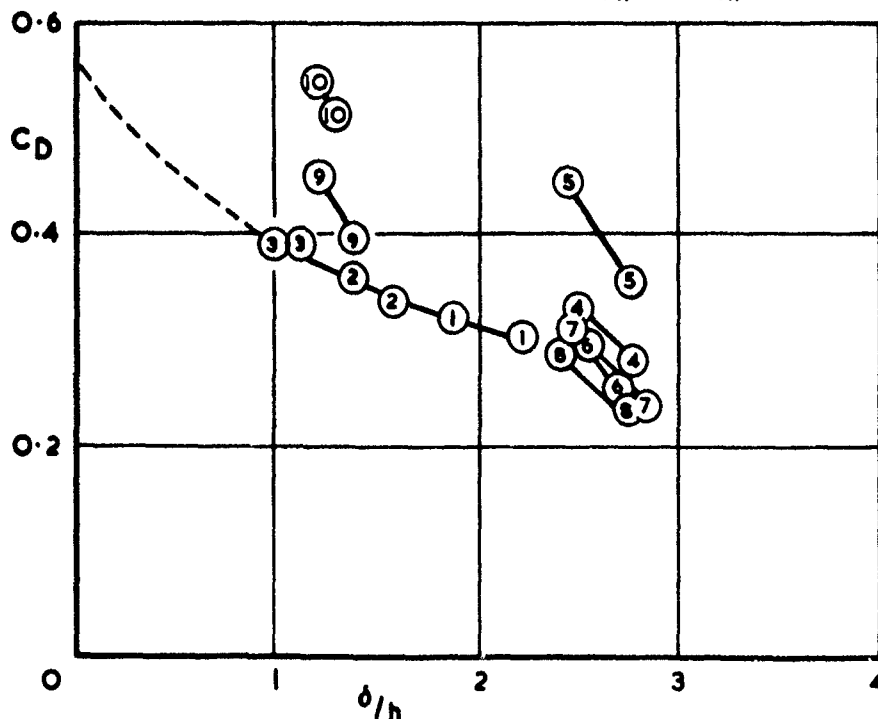
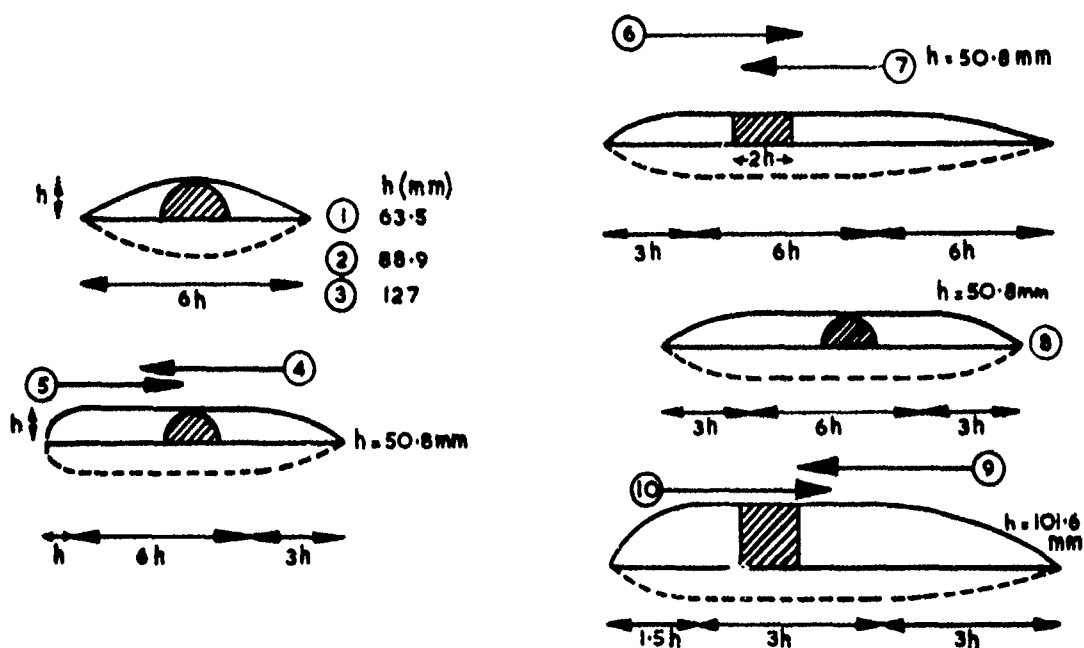


Fig.27 Fairings M=1.4

T. MEMO AERO 1536

Fig.28a

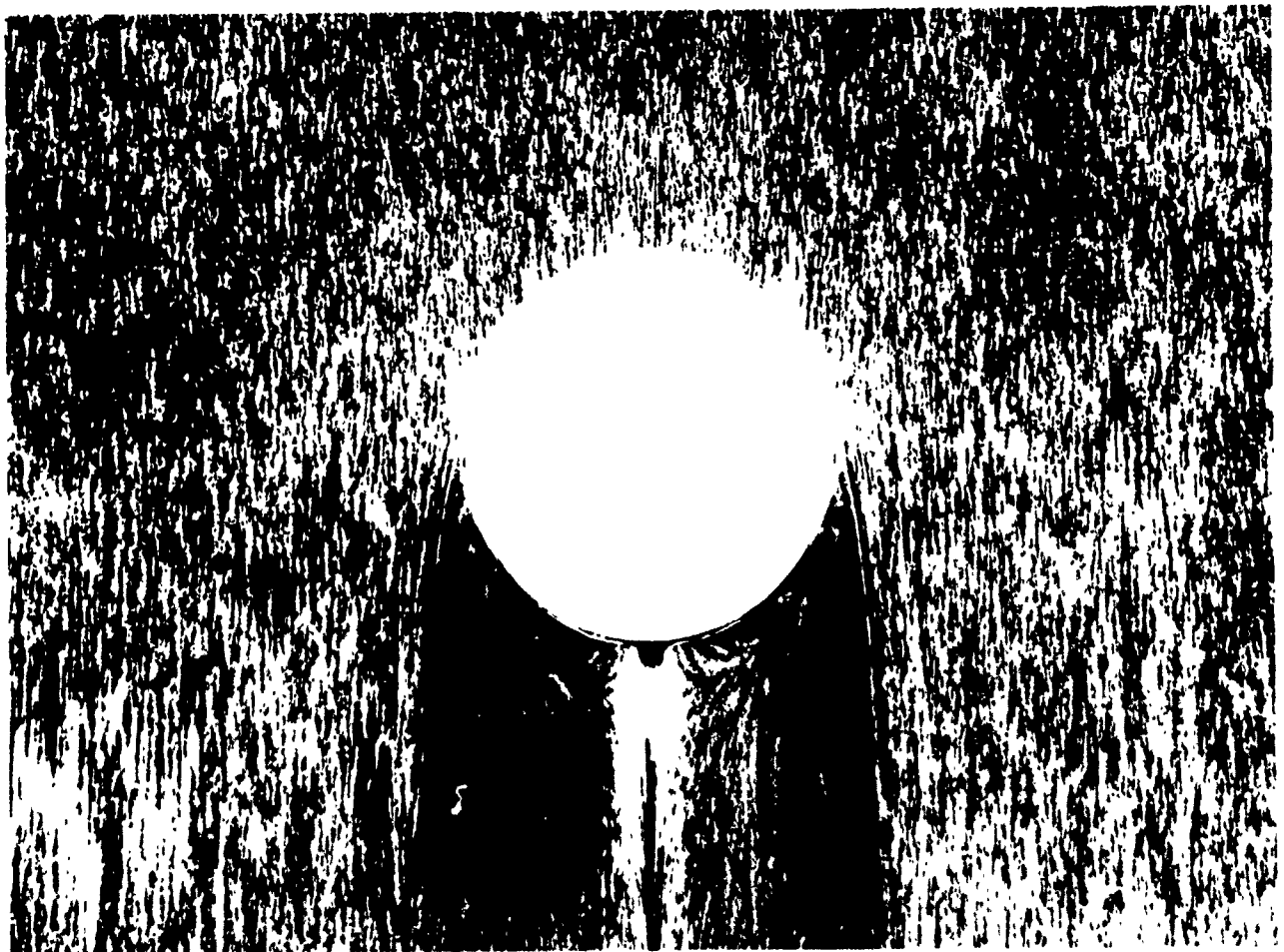
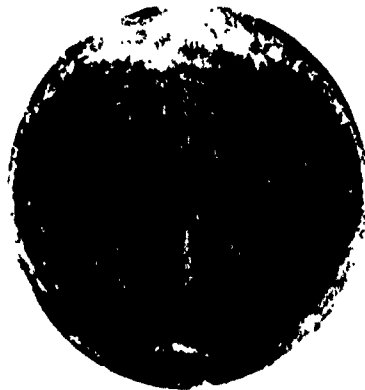
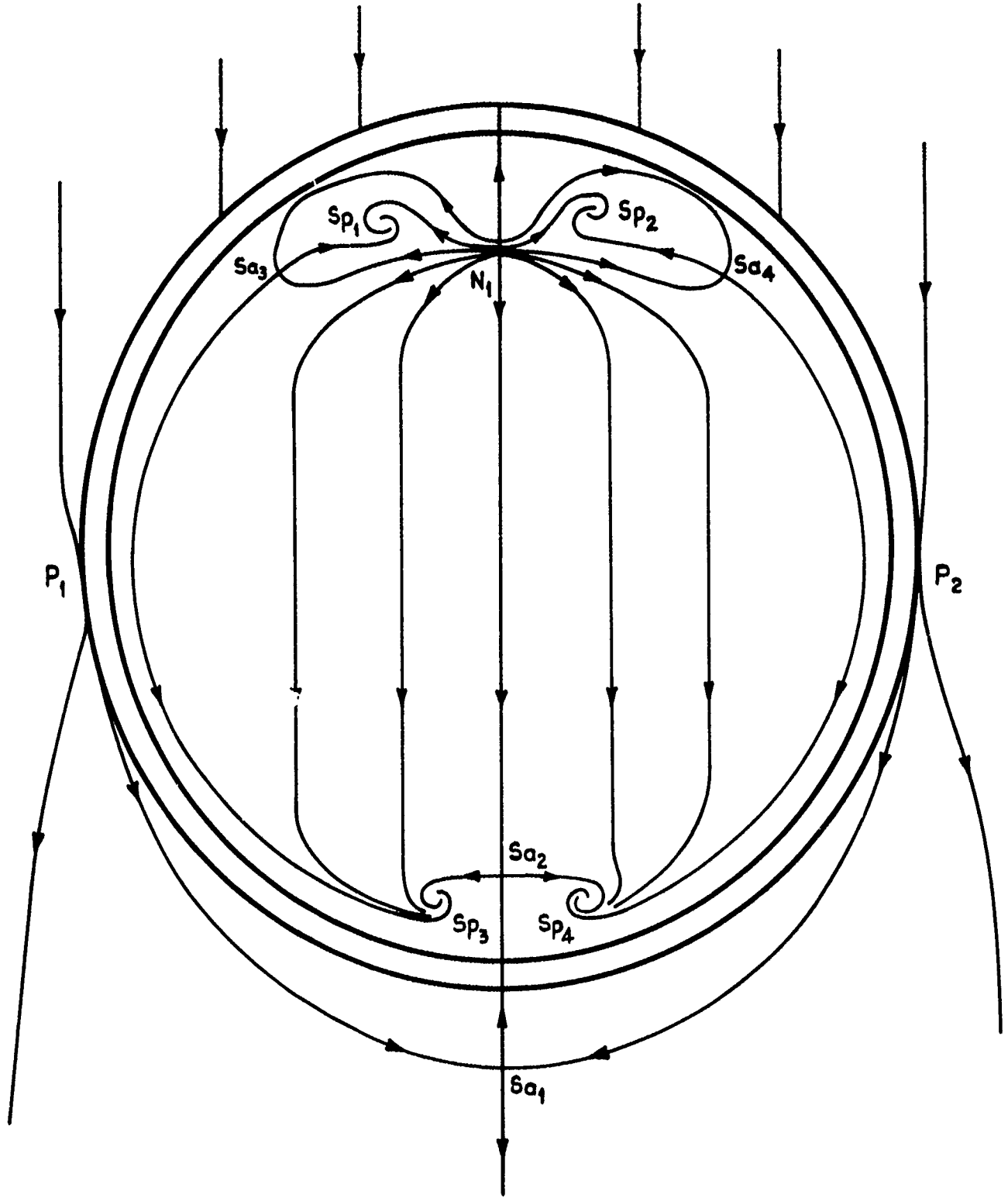


Fig.28a $\frac{h}{d} = 0.04$

T. Memo Aero 1538



$$\frac{\rho}{\mu} = 0.04$$

Fig. 28 b

Fig.29a

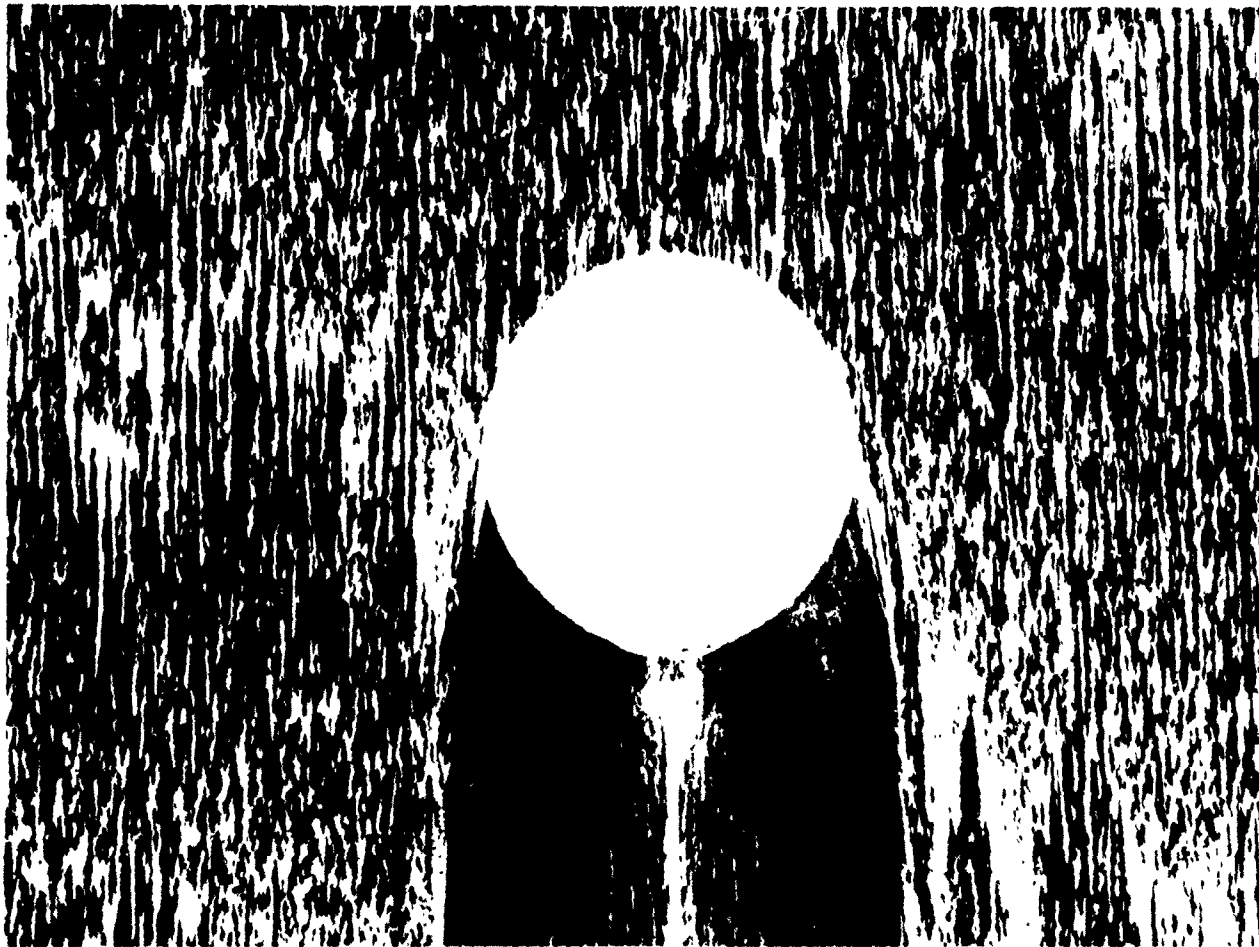


Fig.29a $\frac{h}{d} = 0.09$

Fig.29b

T. Memo Aero 1538

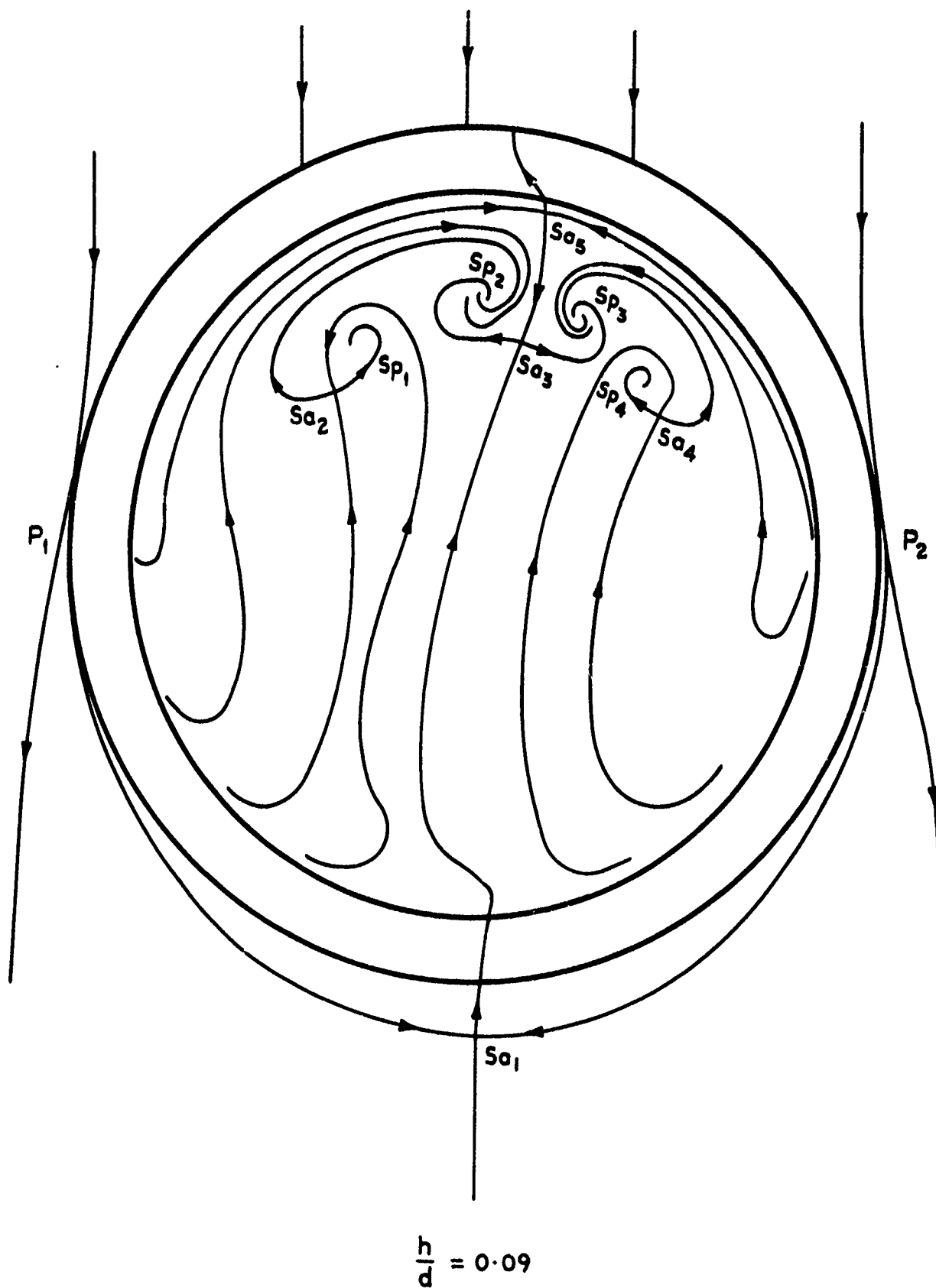


Fig. 29 b

Fig.30a

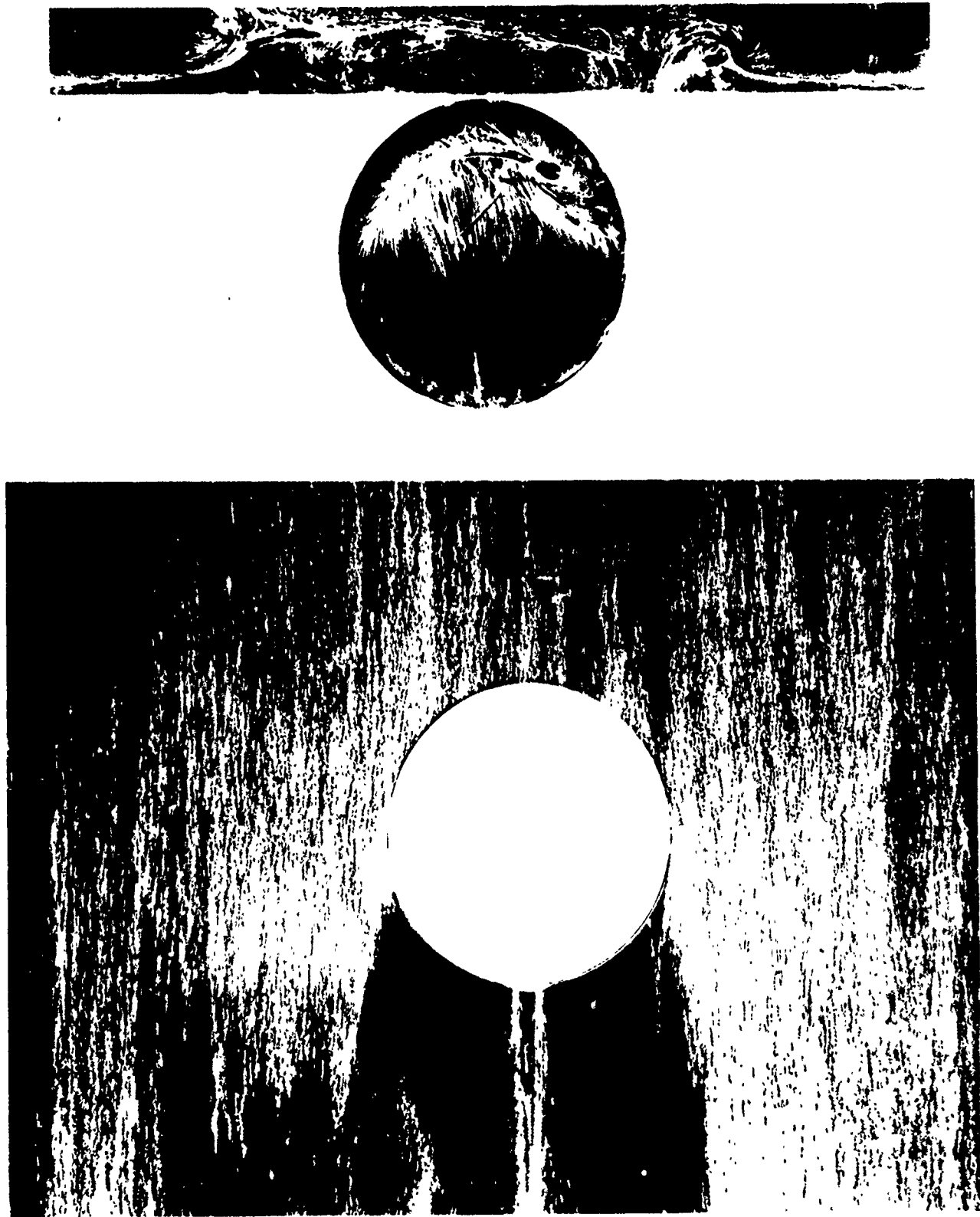
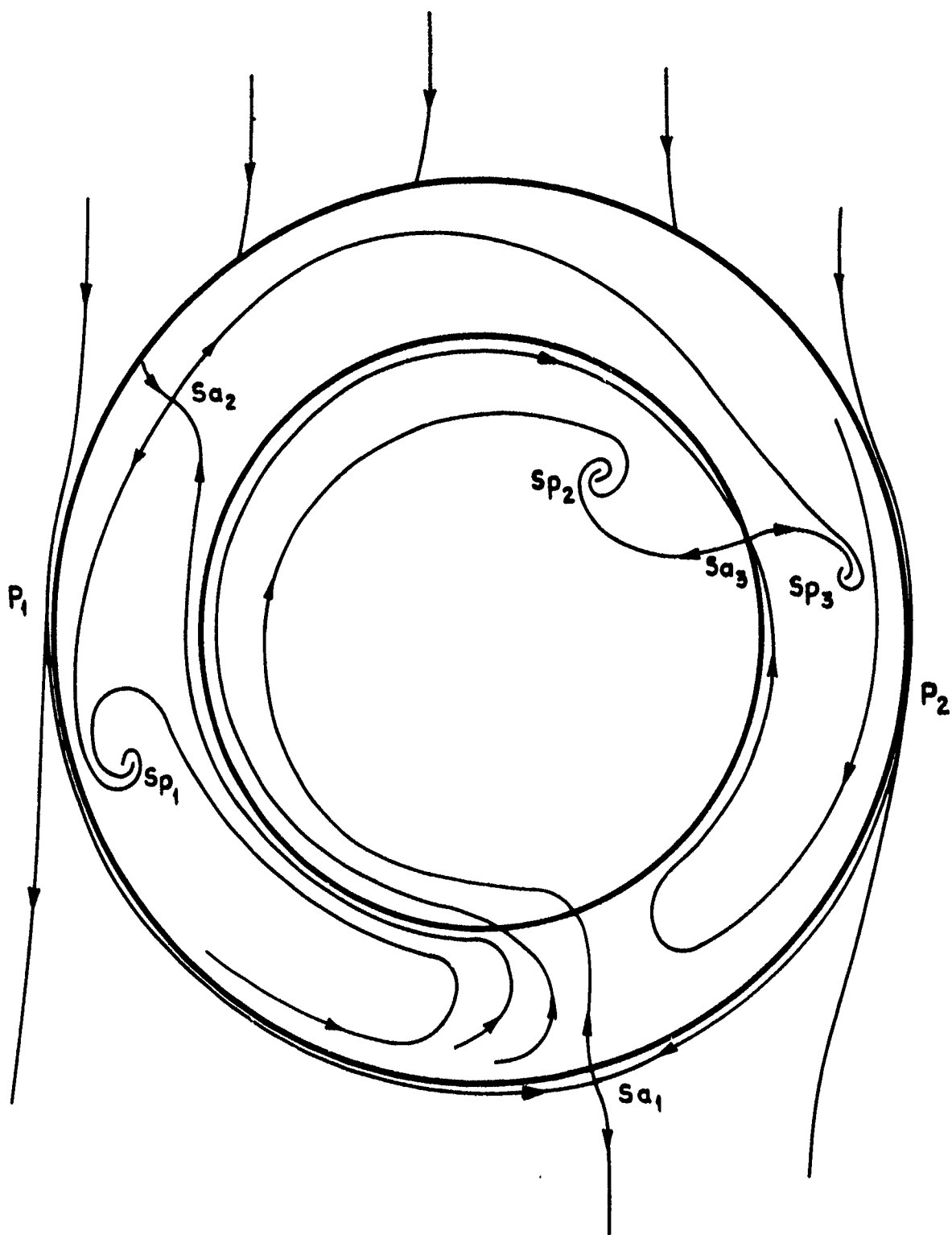


Fig.30a $\frac{h}{d} = 0.29$

Fig. 30 b

T. Memo Aero 1538



$$\frac{a}{r} = 0.29$$

Fig.31a

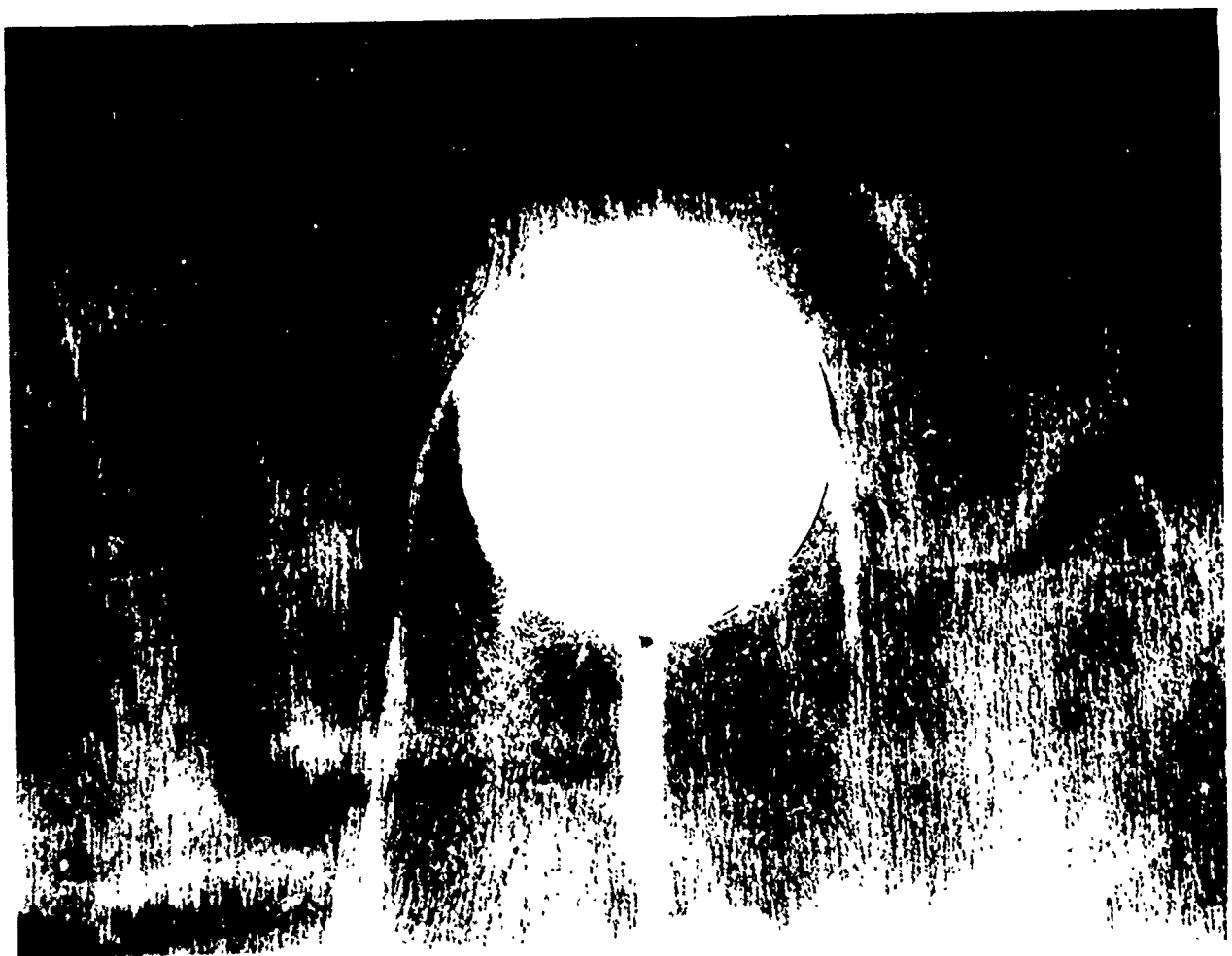
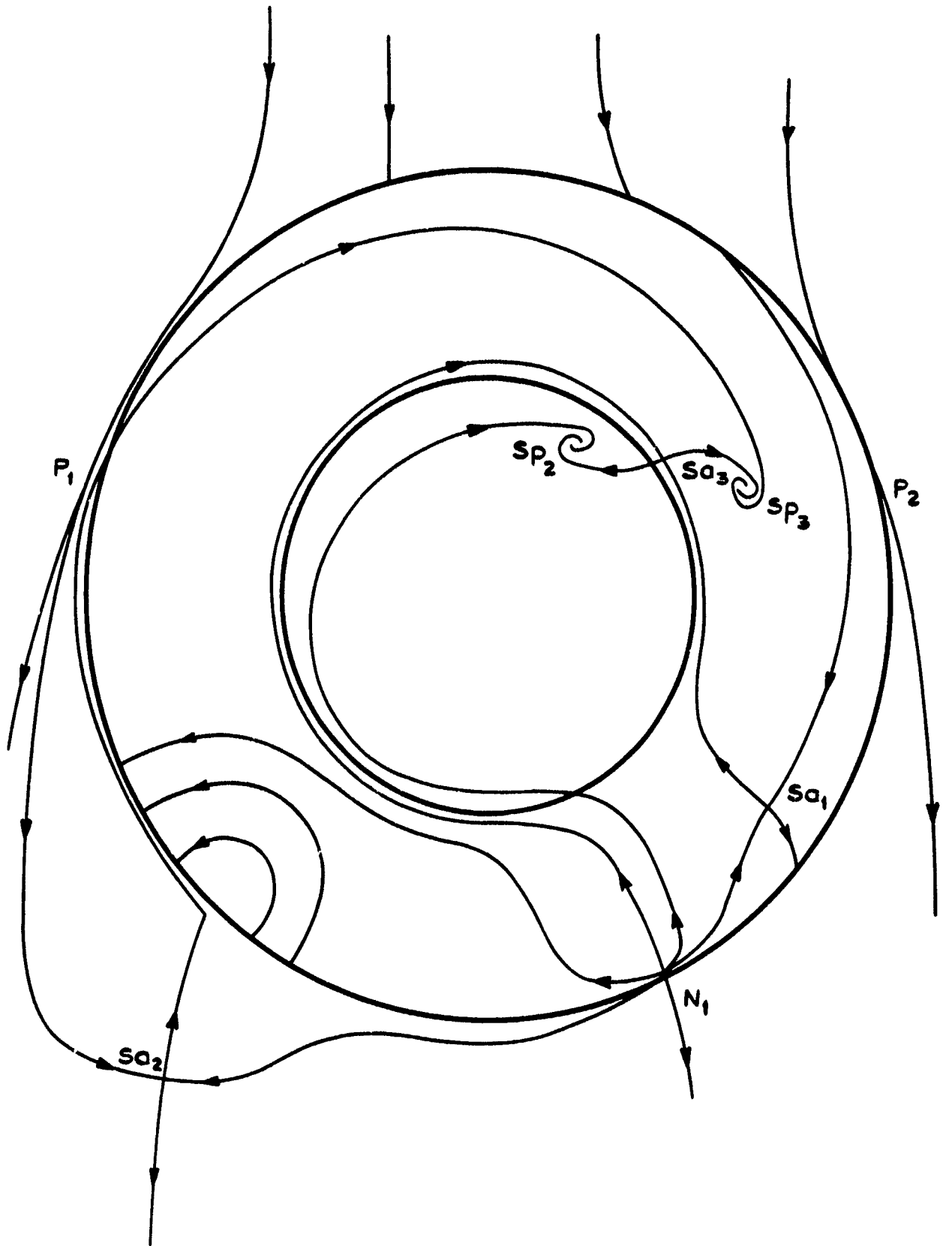


Fig.31a $\frac{h}{d} = 0.47$

Fig.31 b

T. Memo Aero 1538



$$\frac{r}{d} = 0.47$$

Fig.31 b

Fig.32a

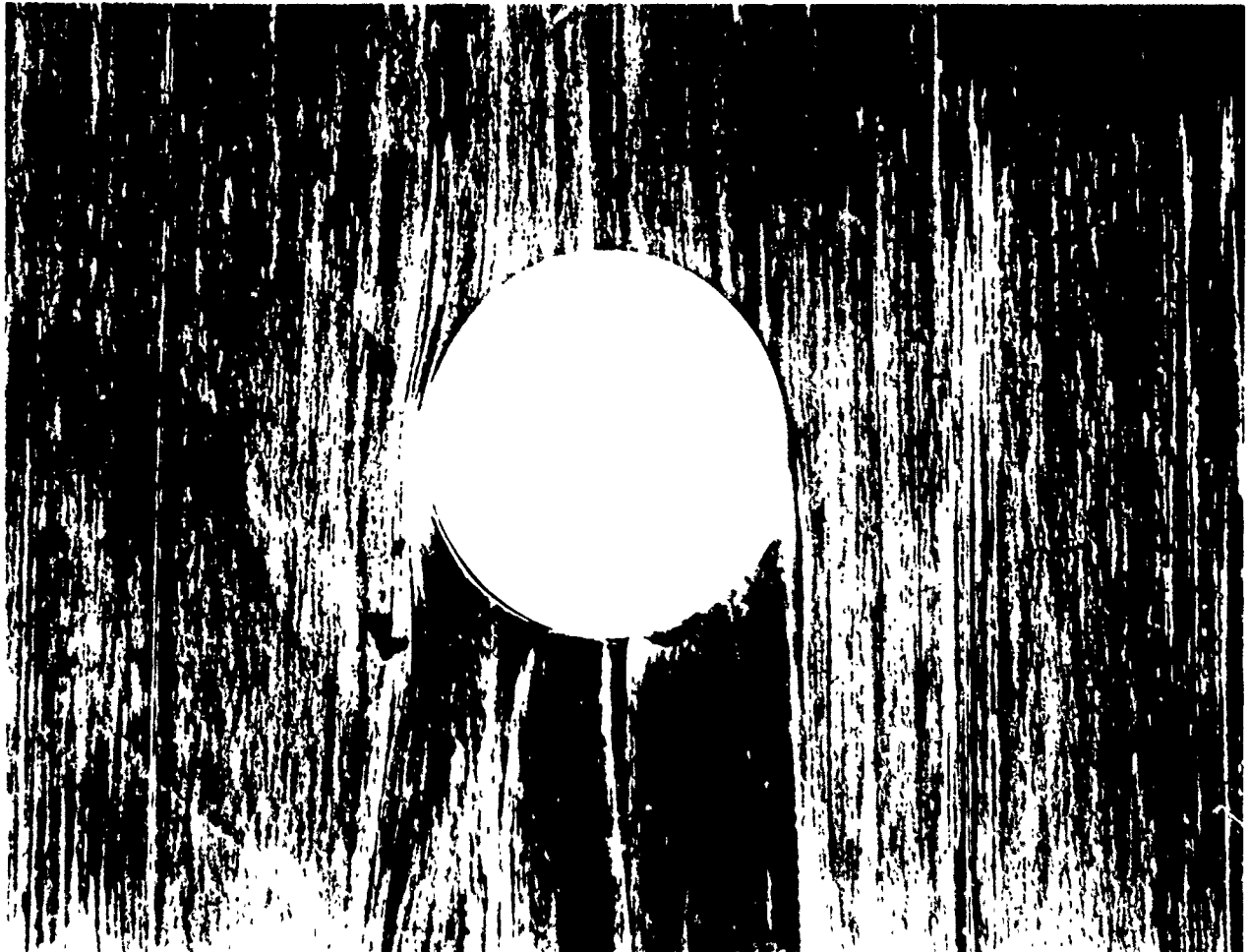
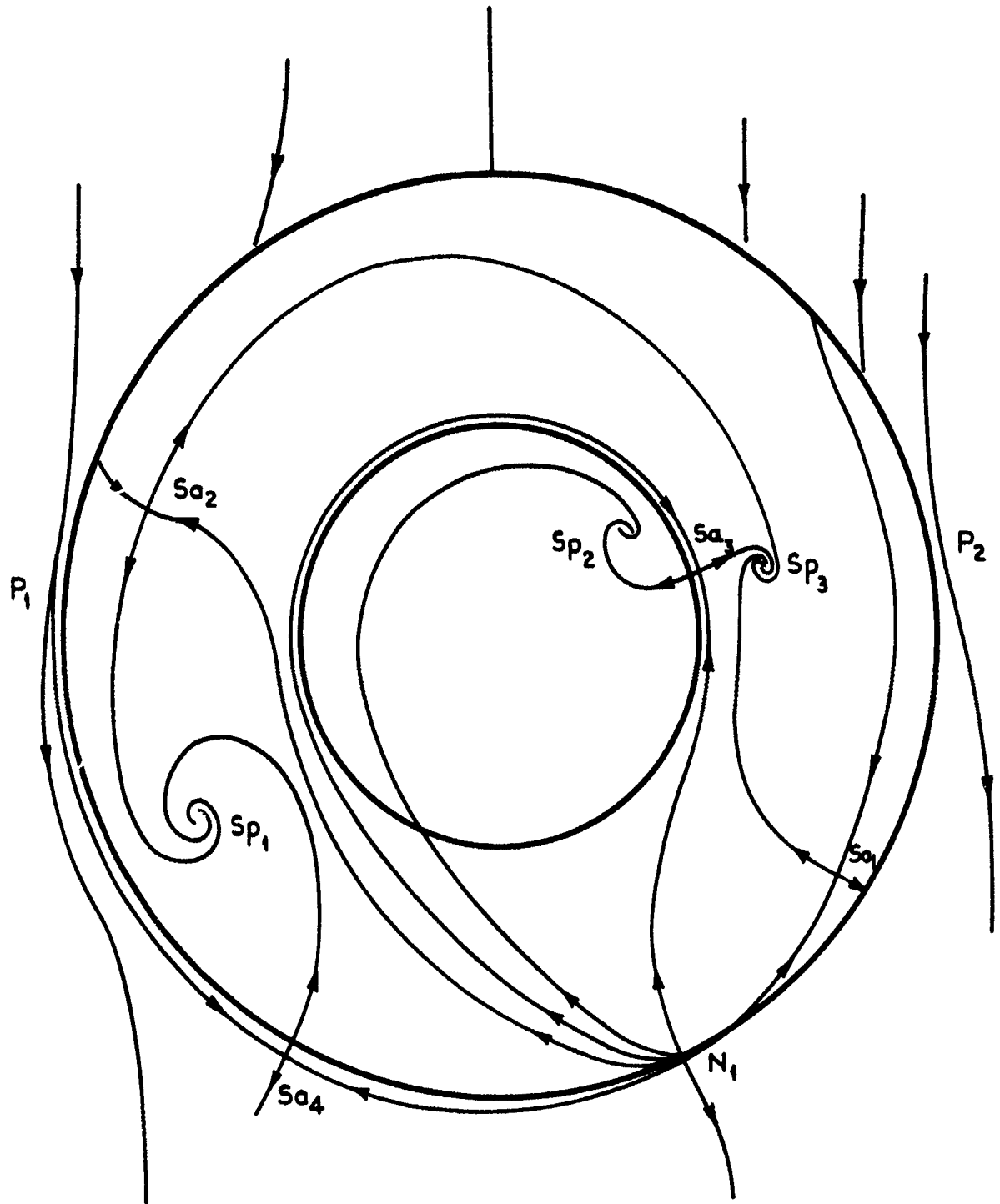


Fig.32a $\frac{h}{d} = 0.60$

Fig.32 b

T. Memo Aero 1538



$$\frac{a}{b} = 0.60$$

Fig. 32 b

Fig.33a

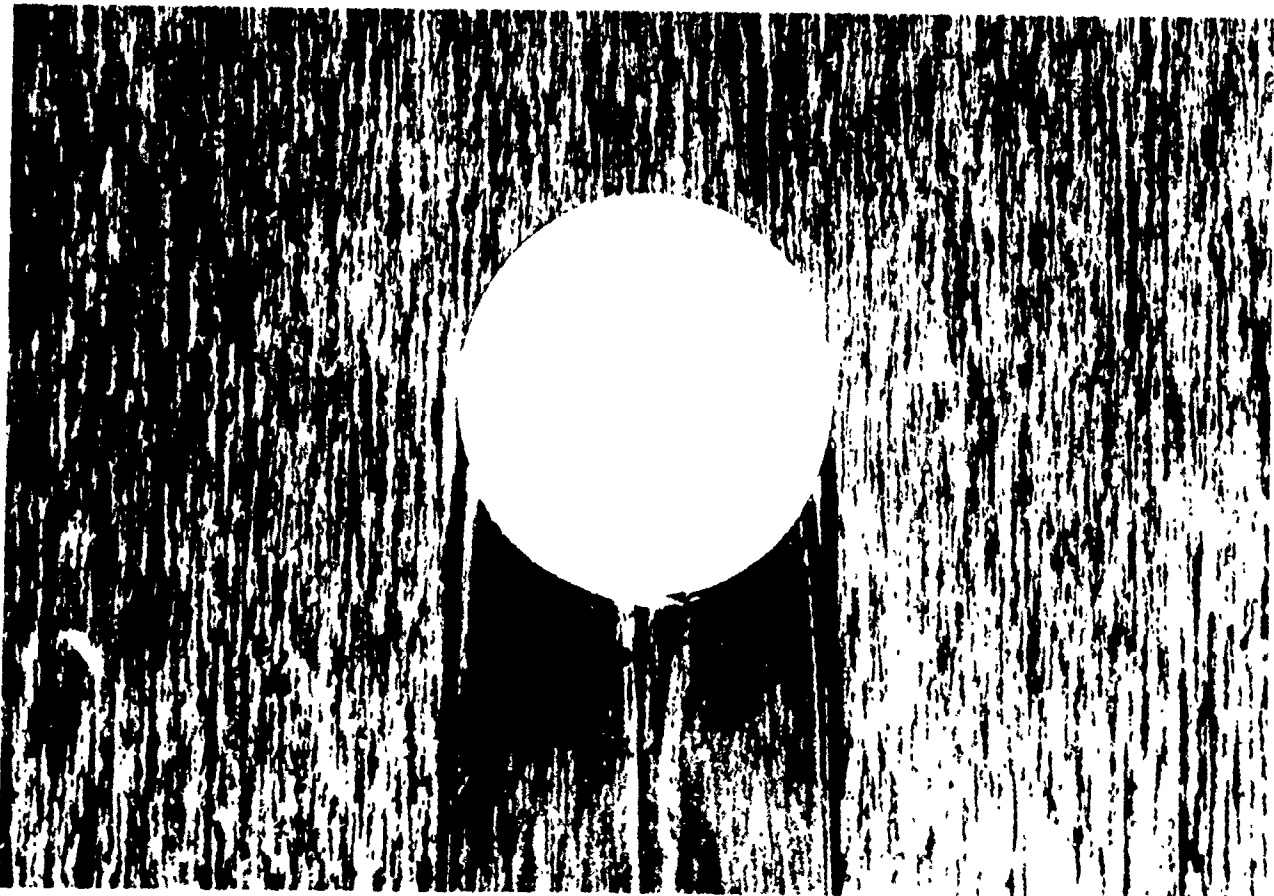
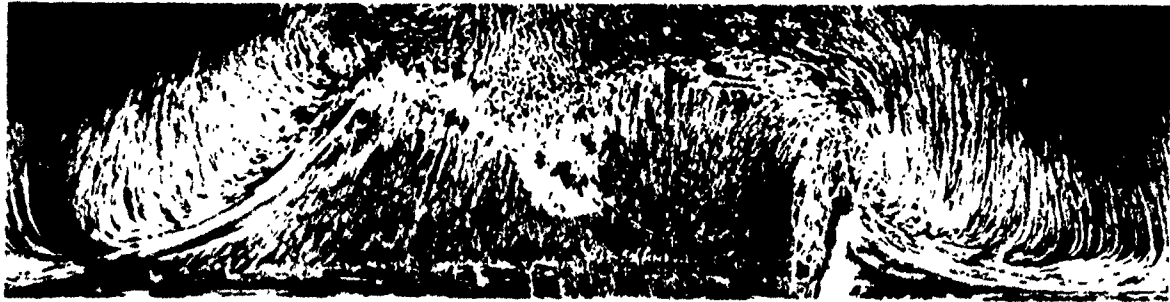
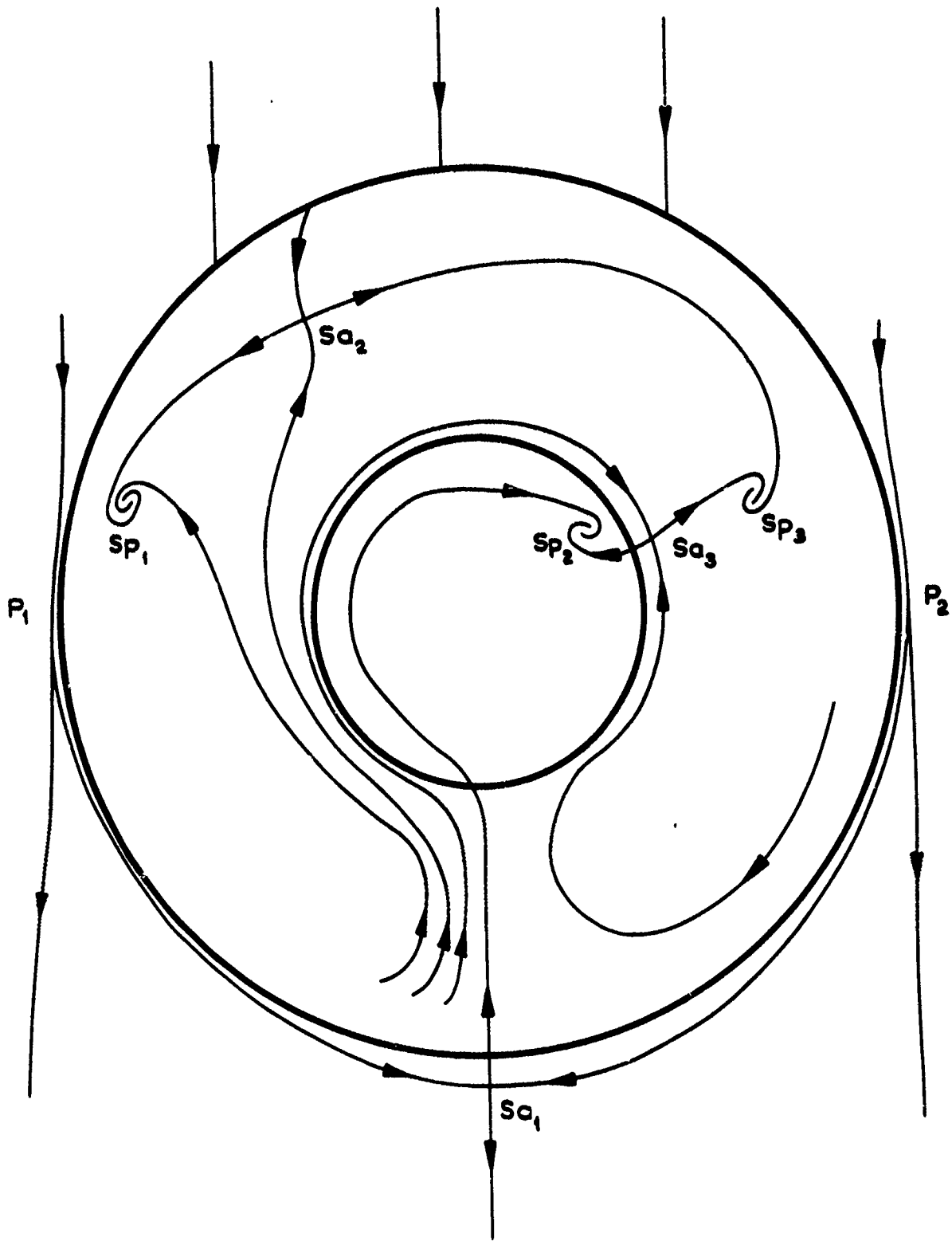


Fig.33a $\frac{h}{d} = 0.78$

Fig.33b



T. Memo Aero 1536

$$\frac{a}{r} = 0.78$$

Fig.34a

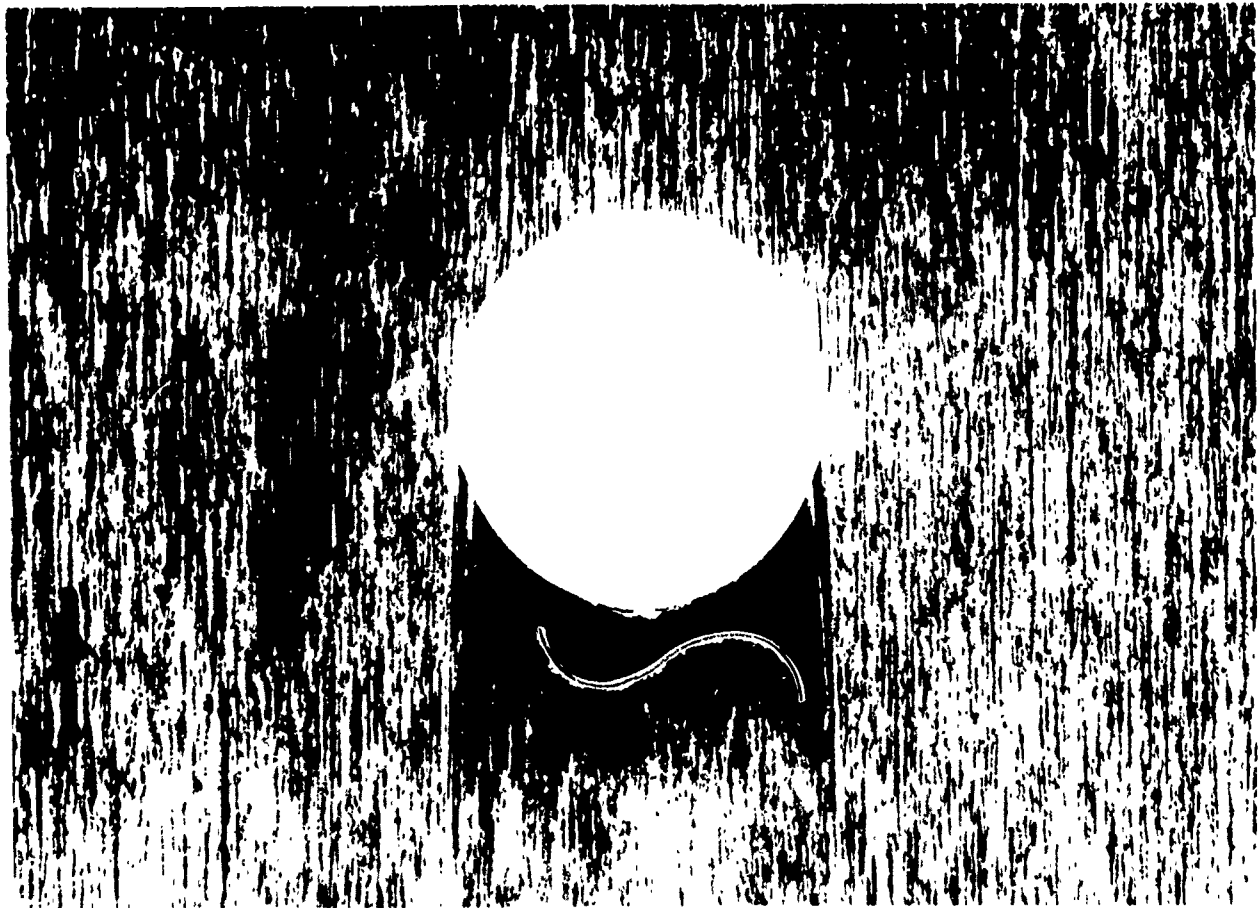
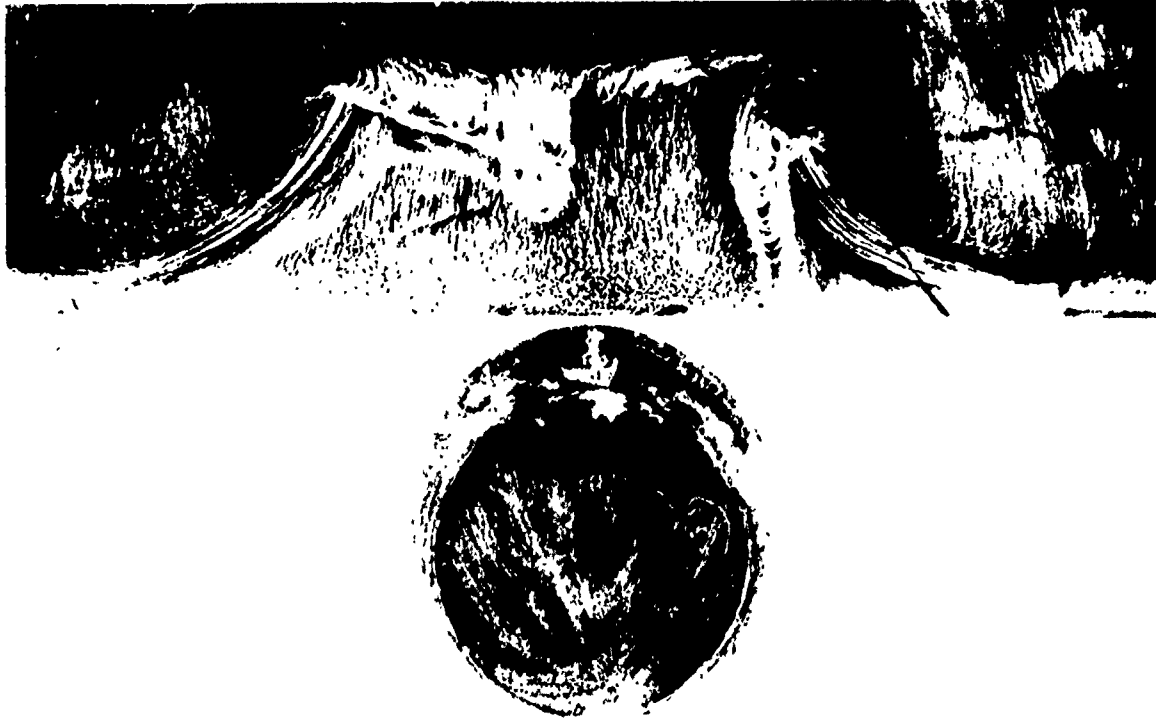


Fig.34a $\frac{h}{d} = 0.86$

Fig.34 b

T. Memo Aero 1538

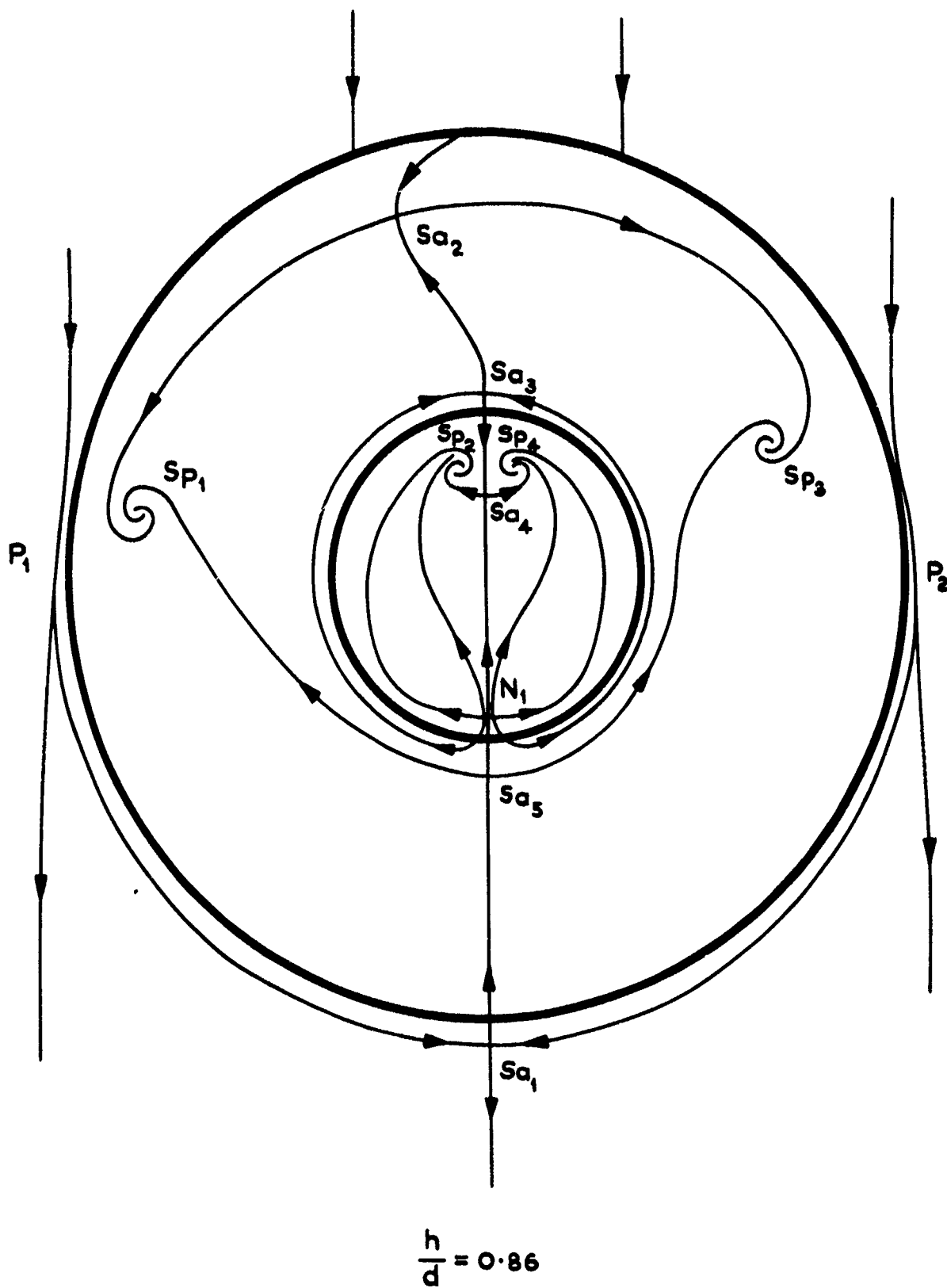


Fig. 34 b

Fig.35a

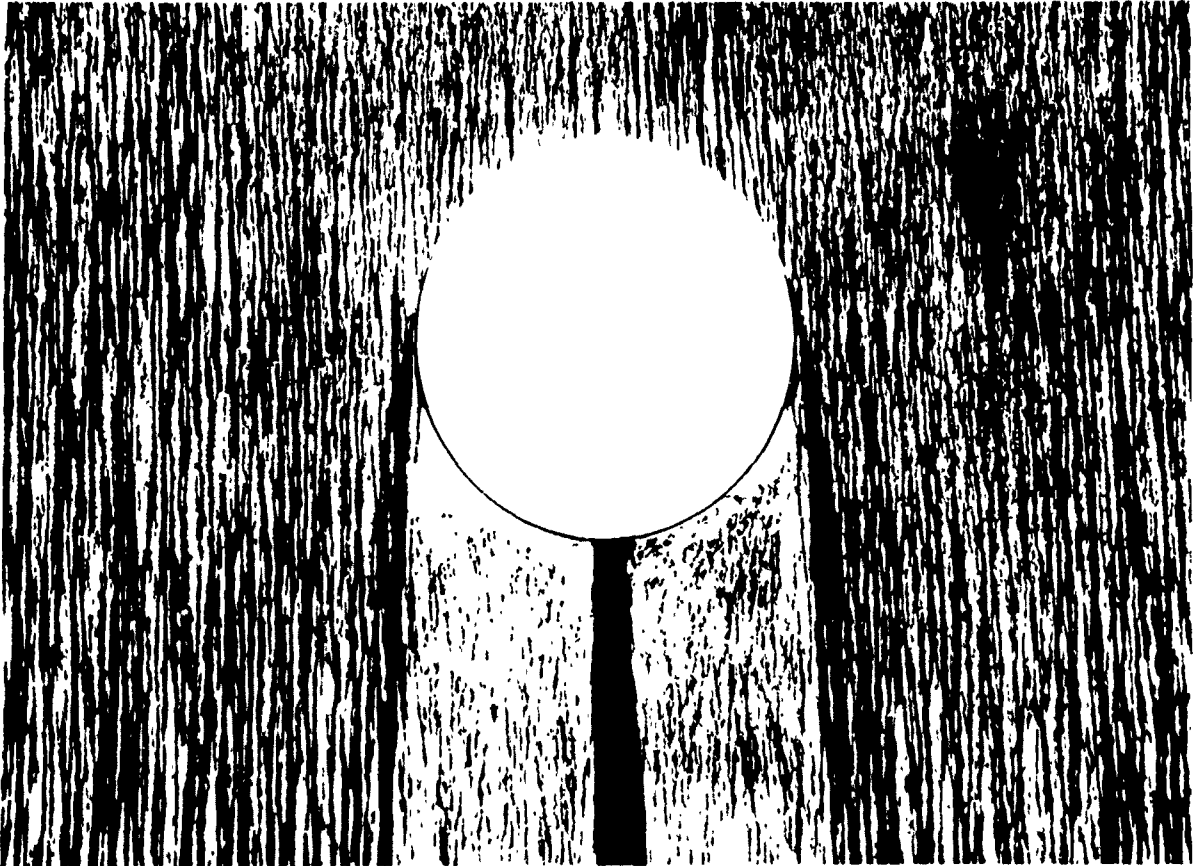
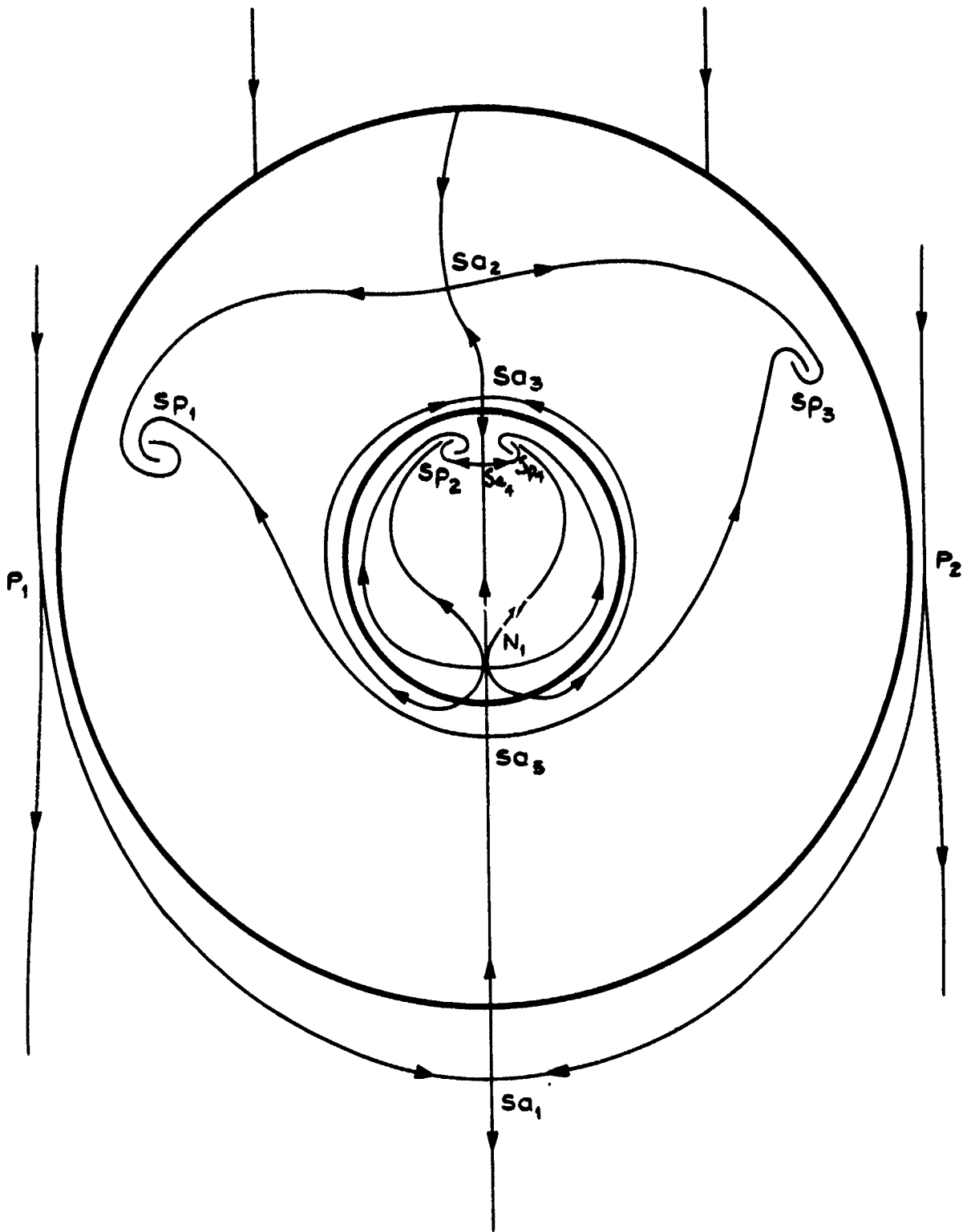


Fig.35a $\frac{h}{d} = 1.07$

Fig.35 b

T. Memo Aero 1536



$$\frac{a}{\gamma} = 1.07$$

Fig.35 b

Fig.36a

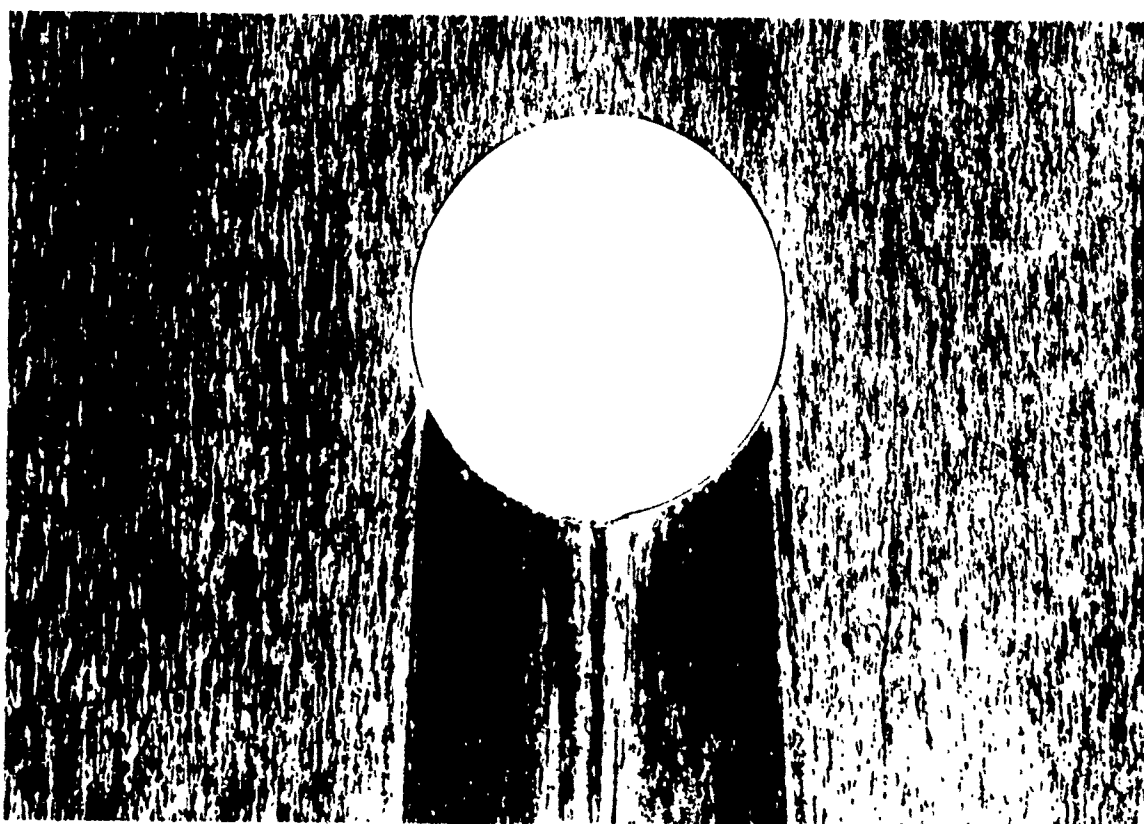
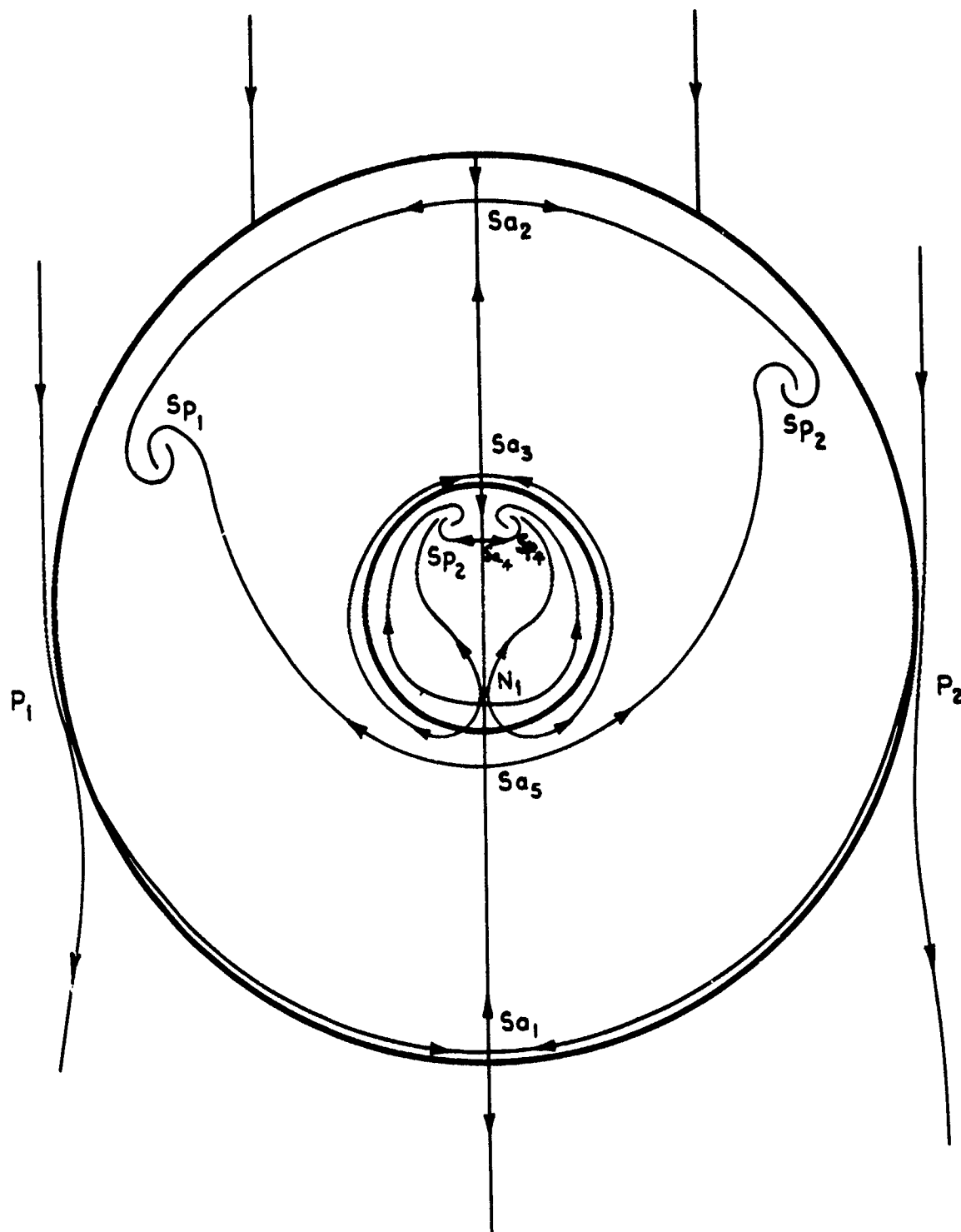


Fig.36a $\frac{h}{d} = 1.34$

T. Memo Aero 1538



$$\frac{v}{a} = 1.34$$

Fig. 36 b



*Information Centre
Knowledge Services*
[dstl] Porton Down,
Salisbury
Wiltshire
SP4 0JQ
22060-6218
Tel: 01980-618753
Fax 01980-618970

Defense Technical Information Center (DTIC)
8725 John J. Kingman Road, Suit 0944
Fort Belvoir, VA 22060-6218
U.S.A.

AD#: AD918999

Date of Search: 17 November 2008

Record Summary: AVIA 6/24552

Title: Measurements of the Drag of some Characteristic Aircraft Execrescences Immersed
in Turbulent Boundary Layers

Availability Open Document, Open Description, Normal Closure before FOI Act: 30 years

Former reference (Department) AERO 1538

Held by The National Archives, Kew

This document is now available at the National Archives, Kew, Surrey, United Kingdom.

DTIC has checked the National Archives Catalogue website (<http://www.nationalarchives.gov.uk>) and found the document is available and releasable to the public.

Access to UK public records is governed by statute, namely the Public Records Act, 1958, and the Public Records Act, 1967.

The document has been released under the 30 year rule.

(The vast majority of records selected for permanent preservation are made available to the public when they are 30 years old. This is commonly referred to as the 30 year rule and was established by the Public Records Act of 1967).

This document may be treated as UNLIMITED.